Computers & Structures, Volume 330, September 2026, Article number 108344
DOI: 10.1016/j.compstruc.2026.108344

Configuration optimization of tuned mass inerter absorbers for cable vibration suppression considering experimentally identified parasitic effects

Sara Ying Zhang[a], Deyuan Li[a], Qi Zhu[a], Haonan He[b,*], Yiyuan Li[c,*]

[a] *School of Electromechanical Engineering, Guangdong University of Technology, Guangzhou*
[b] *College of Aerospace and Civil Engineering, Harbin Engineering University,Harbin*
[c] *Advanced Vehicle Engineering Centre, Cranfield University, Cranfield*

Abstract

Traditional cable vibration control mainly relies on dampers, whose effectiveness is often limited by installation position. Tuned mass dampers can improve performance, but require additional mass. More recently, inerters have been introduced to further enhance vibration mitigation performance, with the tuned mass damper inerter being the most notable example. However, only a limited subset of possible tuned mass inerter absorber layouts – comprising a reaction mass and a number of springs, dampers, and inerters – has been explored. In addition, parasitic nonlinearities in practical implementations are often neglected, leaving their influence on performance prediction unclear. This study presents a systematic synthesis and optimisation framework of tuned mass inerter absorbers for cable vibration control. Generic immittance-function networks are used to generate and evaluate all feasible layouts under the component constraints, while experimentally identified parasitic effects are incorporated. A finite element cable model is developed, and the robustness of the proposed absorber is assessed under seismic and wind loading. The results show that the optimal configuration outperforms conventional tuned mass damper and tuned mass damping inerter, reducing maximum cable displacement by up to 33.1% and 7.9%. The refined design also limits the performance loss caused by parasitic effects to less than 5.4%.

Keywords: Tuned mass inerter absorber, Generic immittance-function networks, Cables, parasitic effects

1. Introduction

The mitigation of stay cable vibrations has attracted wide research interest in recent years due to its significance in the structural performance of cable-stayed bridges[1, 2]. These cables, known for their lightweight, flexibility, and inherently low damping capacity, are highly susceptible to excessive vibrations under a variety of dynamic loads, including seismic excitatons[3] and wind-induced forces[4]. Such vibrations may lead to fatigue damage, cracking, or even failure, posing critical safety threats to the structural integrity of bridges. To address this challenge, a range of vibration control techniques have been developed, including active systems[5], semi-active devices like magnetorheological (MR) dampers[6], and passive energy dissipation mechanisms[7]. Among

*Corresponding author
Email addresses: haonan.he@hrbeu.edu.cn (Haonan He), yiyuan.li@cranfield.ac.uk (Yiyuan Li)

Published by Elsevier. This is the Author Accepted Manuscript issued with: Creative Commons Attribution License (CC:BY 4.0).
The final published version (version of record) is available online at DOI:10.1016/j.compstruc.2026.108344. Please refer to any applicable publisher terms of use.

these, passive control strategies are particularly attractive due to their inherent stability, minimal energy demand, and cost-effectiveness, making them widely adopted in practical engineering applications.

A common utilized passive control device for cable structures is the viscous damper (VD)[8–10], which can compensate for the inherent damping of the cables and improve their modal damping ratio to mitigate deleterious vibrations. The optimal design of the VD for suppressing the rain-wind-induced vibrations of stay cables was proposed in [11], and its control capability was verified through full-scale experiment testing [12], considering the nonlinearity effect. However, the installed position of VDs—normally close to cable ends— significantly limits their control effectiveness [13]. Other damping enhancement methods, such as the semi-active or active devices [14, 15], were subsequently proposed, but the drawbacks, such as higher power requirements and potential instability risks restrict their wide application on cables. As an alternative, the tuned mass damper (TMD) offers a feasible passive vibration control strategy due to its adaptability to any location along the cable. Studies, including those on a flexible cable[16] and the Oresund Bridge cable[17], have demonstrated that TMDs can offer enhanced damping effects compared to the VDs when tuned for specific vibration modes[18], but for multiple modes, the TMD has limited performance advantages [19]. To overcome these limitations, recent studies proposed combining TMDs with VDs to exploit the advantages of both devices and improve overall damping characteristics of cables [20, 21]. This hybrid strategy has been reported to yield better multi-mode suppression and greater damping ratios than individual devices alone[22]. Some other new technologies have also been proposed, such as the negative-stiffness damper [23] and the eddy-current damper [24].

Recently, the inerter - a dynamic component that exerts force based on relative acceleration between its terminals, has been extensively adopted in passive control designs. The inerter based absorbers (IBA), formulated by combining inerters with springs and dampers, have been employed in various civil structures, such as buildings [25], bridges [26] and wind turbines [27], showing significant performance benefits. Hence, it has also been applied to cables by replacing the VD. Lazar et al. [28] first adopted an IBA layout, tuned inerter damper (TID), to suppress cable vibrations under earthquake excitation, suggesting that the TID provides better performance than a traditional VD. The control effectiveness of TID was further verified for cables considering different stiffness connections [29] and girder vibrations [30]. In addition to the TID, other IBA layouts, such as the inertial damper [31, 32] or the inertial mass damper [33, 34] were also proposed for cables, showing the control effectiveness of using inerters. By using a network-synthesis-based method, Luo et al. [35, 36] identify the optimum configuration of inerter-based absorbers for cables, suggesting that the proposed IBA can significantly increase the damping ratio compared to the VD. Gao et al. [37] proposed a negative stiffness inerter damper, providing a significant damping enhancement for stay cables.

Previous studies have confirmed that the inerter based absorbers can effectively enhance the vibration control performance of stay cables. However, similar to conventional viscous damper, their control effectiveness is often restricted by the installation position constraints. To overcome this shortcoming, the inerter-based absorbers can be combined with the TMD, forming passive absorbers consisting of inerters, dampers, springs and a reaction mass, termed as tuned mass inerter absorber (TMIA). By substituting the damper in the TMD with the IBA, Hu et al. [38] proposed four TMIA layouts with one structural attachment point, suggesting that compared

to the traditional TMD, TMIA can provide significant performance improvements for a single-DOF structure. Various structural systems, such as beams[39] and bridges[40], have been used to demonstrate the effectiveness of such TMIA configurations. Beyond single-attachment designs, Marian and Giaralis [41] proposed a TMIA layout with two structural attachment points by connecting an inerter in series with a TMD, which is termed as the TMDI. Subsequent studies further investigated TMDI systems on buildings under seismic excitations, controller optimization, and soil–structure interaction effects [42–44]. Notably, the TMDI has been shown to outperform the IBA-type absorber, the TID for buildings [45] and traditional TMD for beams when properly optimized [46]. Recent studies have further expanded the application of TMDIs by considering soil–structure interaction effects, multi-hazard wind–seismic excitations and nonlinear behaviour [47–51]. These investigations have demonstrated the effectiveness of TMIA-type systems in enhancing structural vibration mitigation under a wide range of loading and operating conditions. Nevertheless, the majority of existing studies focus on a limited number of predefined absorber layouts, while the broader range of potential TMIA configurations has received comparatively little attention.

The significant advantages reported for these TMIA systems highlight the merits of employing mass-inclusive designs that incorporate all three two-terminal mechanical elements – inerters, dampers and springs. Given the numerous possible interconnections among these elements, a large design space of TMIA configurations exists, potentially offering different levels of vibration mitigation performance. However, the potential benefits of adopting TMIA-type absorbers to mitigate cable vibrations have yet to be thoroughly addressed. This work aims to extend the successful application of TMIA into stay cables, exploring the potential vibration suppression performance benefits. To this end, a systematic methodology based on the generic immittance-function networks [52] and the structure-immittance approach [53] is used, facilitating comprehensive exploration across all possible candidate layouts with a reaction mass and pre-determined number of springs, dampers and inerters. By modelling the cable as a finite element system and maximising the damping ratio around the first fundamental frequency, the optimal TMIA configurations—featuring one or two structural attachment points—are identified. The effectiveness of the proposed designs is then assessed through numerical simulations under various external excitations, including seismic and wind loads.

Typically, the spring and damper in vibration absorbers exhibit predominantly linear characteristics due to their simple structures. However, the practical implementation of an inerter often introduces significant nonlinearities such as friction and parasitic damping effects. Therefore, it is essential to investigate the vibration suppression effectiveness of inerter-based devices considering the physical realisation. In Smith's original design [54], the primary realizations of inerter include the ball-screw type [55], rack-and-pinion type [56], and fluid inerter [57, 58]. The fluid inerter, designed based purely on hydraulic principles, offers advantages such as high load-bearing capacity and fast response speed. It simultaneously avoids issues inherent to mechanical inerters, like transmission backlash and impact wear, making it a promising direction for the next generation of inerter development. Chillemi et al. experimentally validated the vibration reduction performance of fluid inerters [59, 60]. Shen et al. demonstrated the application of fluid inerters in suspension systems through experimental testing [61]. Concurrently, these experimental studies indicate that fluid inerters face significant

nonlinear factors in practical applications, which need to be identified and mitigated through optimization. To accurately characterize the parasitic effects of fluid inerters and describe their impact on the vibration suppression performance of cables, this study further conducts a systematic performance investigation through experimental and numerical analyses.

This paper is organized as follows. A cable model established by means of finite element method is presented in section 2, where the performance measure is also proposed. Section 3 formulates the generic immittance-function networks for enumerating all the candidate TMIA layouts with the structure-immittance approach. Optimum absorber configurations are achieved in Section 4, and the absorber robustness with respect to the change of parameter values and installation positions is checked. Performance verification is also carried out by subjecting the cable model to both the earthquake excitation and wind loads. Section 5 focuses on control effectiveness of the proposed absorber considering the physical realisation, where the parasitic effects of the fluid inerter is identified and the absorber design is refined. Conclusions are drawn in section 6.

2. Mathematical model and performance measure

The development of a finite element model for the cable system is presented in this section, incorporating a combined implementation of a viscous damper and a tuned mass inerter absorber (TMIA) for vibration control. The modal damping ratio is adopted as the primary metric to assess vibration mitigation effectiveness. Subsequently, the absorber parameters are nondimensionalized, and the model is validated by comparing the numerical results with those reported in [35].

2.1. Cable model with a damper and a tuned mass inerter absorber

Consider a cable with the total mass of M and the total length of L, its first mode undamped natural circular frequency is given by:

$$\omega_0 = \pi\sqrt{T/(ML)} \tag{1}$$

where T represents the tension of the cable. Using the finite element method, the cable is discretized into an (n)-DOF lumped-mass model, as illustrated in Fig. 1. Since the primary objective of this work is to develop a systematic synthesis and optimisation framework for TMIA configurations rather than to establish a high-fidelity cable model for a specific bridge, a simplified tension-dominated in-plane cable model is adopted. In this model, effects such as cable sag, cable curvature, out-of-plane deformation, additional material-elasticity effects, and inherent cable damping are not explicitly considered. These assumptions are commonly adopted in previous cable vibration control studies [28, 35, 36], and allow different TMIA topologies and parameter combinations to be efficiently assessed while maintaining computational efficiency. The adopted model is most applicable to tension-dominated cables undergoing relatively small-amplitude vibrations, where the dynamic response is governed primarily by the first few in-plane modes.

In the model shown in Fig. 1, the cable is represented by n number of masses m distributed along its span, as well as two half-masses $m/2$ at each boundary directly attached to the supports. The total mass is thus

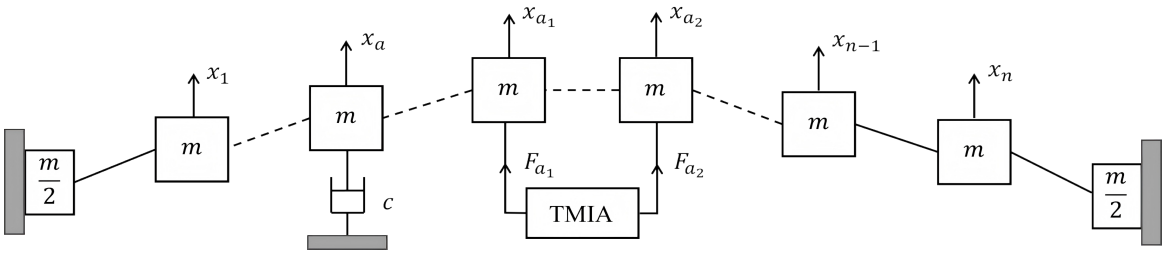

Figure 1: A finite element model of cable with a VD and a TMIA.

divided into $m = M/(n+1)$, and the element length becomes $l = L/(n+1)$. The ith mass element has sociated vertical displacement x_i with equilibrium at $x_i = 0$. The viscous damper c is connected to the ath element, and the tuned mass inerter absorber is assumed to be installed to the cable with two attachment points, exerting forces F_{a1} and F_{a2} on the mass elements a_1 and a_2, respectively. Note that the TMIA can also be attached to one mass element of the cable, which can be analysed by making one of the forces being zero. In this study, a lumped model with $n = 99$ DOFs is adopted, following [35, 36], where the maximum relative difference in the equivalent damping ratio between the 99-DOF and 999-DOF lumped-mass models was reported to be less than 0.1% for modes below $6.5\omega_0$. Based on the model shown in Fig. 1, the equation of motion for each mass element can be obtained as Eq. (2) in Laplace domain.

$$\frac{1}{n+1}s^2\tilde{x}_i + (n+1)\cdot(\frac{\omega_o}{\pi})^2\cdot(2\tilde{x}_i - \tilde{x}_{i-1} - \tilde{x}_{i+1}) = -(\delta_{i,a}\cdot\frac{c}{M}\cdot s\cdot\tilde{x}_a + \delta_{i,a_1}\cdot\frac{\tilde{F}_{a_1}(s)}{M} + \delta_{i,a_2}\cdot\frac{\tilde{F}_{a_2}(s)}{M}) \tag{2}$$

with $\tilde{x}_i(s)$ being the displacement of ith mass in the Laplace domain and δ representing the Kronecker delta function; by defining the displacement vector as $\mathbf{X} = [\tilde{x}_1, \tilde{x}_2, \tilde{x}_3, ..., \tilde{x}_n]^T$, the dynamic equations of the cable can be represented in the matrix form as:

$$(\mathbf{M}s^2 + \mathbf{C}s + \mathbf{K})X + \mathbf{F} = \mathbf{0} \tag{3}$$

where the mass matrix $\mathbf{M}$ is the diagonal matrix of order n, with $1/(n+1)$ as elements. The damping matrix $\mathbf{C}$ is a $n \times n$ matrix with the element c_{aa} equal to c/M and the others being zero, since the present study assumes negligible inherent cable damping, which is in line with the previous works [28, 35]. And the stiffness matrix $\mathbf{K}$ is:

$$\mathbf{K} = \begin{bmatrix} 2\cdot k & -k & 0 & \cdots & 0 & 0 & 0 \\ -k & 2\cdot k & -k & \cdots & 0 & 0 & 0 \\ \vdots & \vdots & & \ddots & & \vdots & \vdots \\ 0 & 0 & 0 & \cdots & -k & 2\cdot k & -k \\ 0 & 0 & 0 & \cdots & 0 & -k & 2\cdot k \end{bmatrix} \tag{4}$$

in which $k = (n+1)\cdot(\omega_0/\pi)^2$. In addition, $\mathbf{F}$ is a $n \times 1$ matrix with each element as $(\delta_{i,a_1}F_{a_1} + \delta_{i,a_2}F_{a_2})/M$, representing the forces exerted by the TMIA. It is worth mentioning that TMIA can also be attached to one

mass element with one of the F_{a_1} and F_{a_2} equal to zero.

2.2. Performance measure and model validation

The issue of cable vibration control has been extensively explored in previous research. Consistent with the findings in [62], this study focuses on enhancing the modal damping ratio to address the inherently low internal damping of cables. It is well recognized that the lowest natural frequency (typically Mode 1) is most vulnerable to vibration amplification [63]. Therefore, the objective of this work is to increase the damping ratio of modes with frequencies close to the fundamental one, while ensuring that the damping performance of higher modes is not inferior to that of a cable using a viscous damper only.

Following the performance measure adopted in previous cable vibration control studies [35, 36], the target frequency range is selected as $\omega_i \in (0, 1.5\omega_0)$. The upper bound of $1.5\omega_0$ is chosen to ensure that, in addition to the fundamental cable mode, any nearby mode introduced by the absorber is also included in the optimisation process. In addition, to prevent deterioration of higher-mode performance, damping constraints are imposed on modes whose natural frequencies lie within the range $\omega_i \in (1.5\omega_0, 4.5\omega_0)$. This follows the same philosophy as previous studies [35, 36], where the damping performance outside the primary optimisation range is also constrained to ensure that the absorber does not compromise higher-mode vibration mitigation. Accordingly, the optimization objective is to maximize the minimum damping ratio within the specified target frequency range $\omega_i \in (0, 1.5\omega_0)$, denoted as ζ_m, and all modes within the frequency range $\omega_i \in (1.5\omega_0, 4.5\omega_0)$ should not have a lower damping ratio than those achieved by an optimised VD.The resulting optimisation problem can be expressed as follows:

$$\begin{cases} \max\ \zeta_m \\ \zeta_m = \min(\zeta_i) \text{ for } \omega_i \in (0,\ 1.5\omega_0) \\ \zeta_i \geq \zeta_{ic} \text{ for } \omega_i \in (1.5\omega_0,\ 4.5\omega_0) \end{cases} \tag{5}$$

where ζ_i represent the damping ratio of the ith mode, ζ_{ic} is the damping ratio with an optimised VD only, and ω_i is the corresponding ith natural frequency. For the cable model, these can be calculated as:

$$\zeta_i = -\frac{\mathrm{Re}(\lambda_i)}{\sqrt{\mathrm{Re}(\lambda_i)^2 + \mathrm{Im}(\lambda_i)^2}}, \quad \omega_i = \sqrt{\mathrm{Re}(\lambda_i)^2 + \mathrm{Im}(\lambda_i)^2} \tag{6}$$

with $\lambda_i (i = 1, 2, 3, ...)$ being the complex eigenvalues of Eq. (3).

To verify the numerical implementation of the cable model and the performance measure adopted in this work, the benchmark example reported in [35] is reproduced. Following [35], only a viscous damper is installed at a location corresponding to 5% of the cable length, with no TMIA attached, i.e. $F_{a1} = F_{a2} = 0$. The minimum damping ratio ζ_m within the frequency range $\omega_i \in (0, 1.5\omega_0)$ and the corresponding natural frequency ω are calculated using Eq. (6) and compared with the results reported in [35]. Here, following [35], we use the non-dimensional damping coefficient c' with the expression $c' = (c/M)/(\omega_0/\pi)$ to represent the damping c and the natural frequency is also nondimensionalized as $\omega' = \omega/\omega_0$. The results suggest that the present model agrees very well with the previous work. In addition, as shown in Fig. 2(a), for the default cable system with a

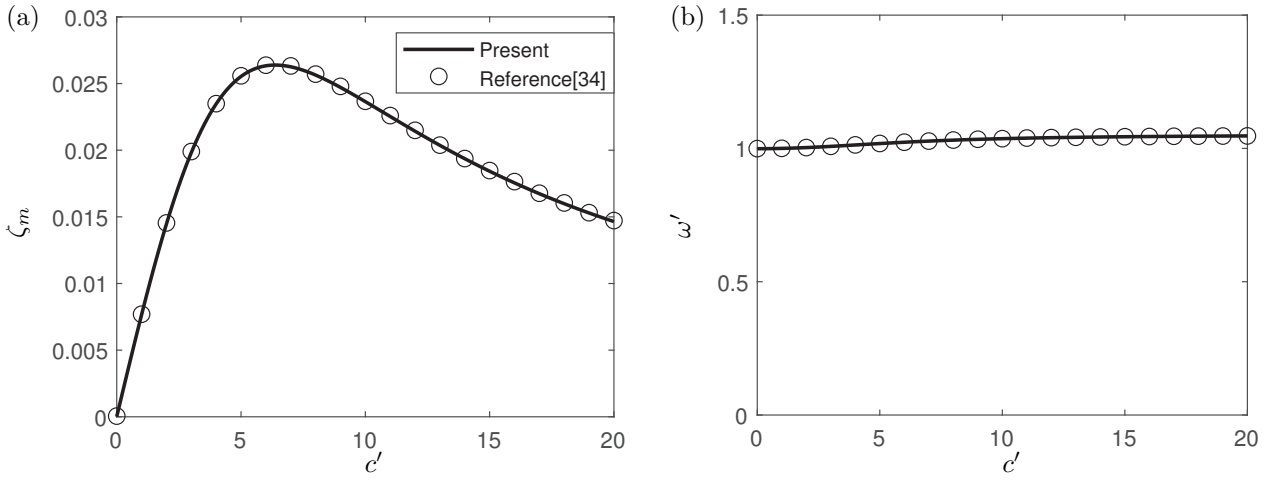

Figure 2: Comparison of (a) minimum damping ratio ζ_m and (b) corresponding natural frequency ω' with respect to the damping coefficient c'.

single viscous damper, the optimal dimensionless damping coefficient is determined to be $c' = 6.35$, resulting in the minimum damping ratio as $\zeta_m = 0.0263$. With the optimum damping coefficient, the damping ratio of the cable modes with $\omega_i \in (1.5\omega_0, 4.5\omega_0)$ can also be calculated using Eq. (6), which can be used as constraints for further optimization.

3. Candidate absorber layouts using generic Immittance-Function Networks

The tuned mass inerter absorbers, consisting of inerters, dampers, springs and a reaction mass, have countless layouts, which could potentially provide preferred vibration suppression performance. In this section, a systematic approach proposed in [52] is adopted to enumerate the candidate layouts of TMIA. Using this approach, the generic immittance-function networks (IF networks), with the ability to cover all layout possibilities, are firstly formulated and subsequently used for further optimisation. Also considering the design simplicity, the TMIA in this analysis is restricted to have a reaction mass and one each of two-terminal element (i.e. the inerter, damper and spring). Furthermore, since the absorber can be installed to the cable with one attachment point (1-AP) or two attachment points (2-AP), the candidate layout enumeration is carried out for two cases, i.e. the 1-AP TMIA and the 2-AP TMIA.

3.1. 1-AP TMIA layouts

Consider the absorber with one attachment point, one typical example is the tuned mass damper, shown in Fig. 3(a), and the TMIA layouts with 1-AP can be represented using the generic immittance-function network illustrated in Fig. 3(b). In this network, the transfer function $Y(s)$ represents the mechanical immittance of the absorber network consisting of one spring, one damper and one inerter. It characterises the dynamic relationship between the force transmitted through the absorber and the corresponding relative velocity at its terminals, and is defined as $Y(s) = F(s)/v(s)$. By representing the absorber using a unified immittance function, different combinations of these three elements can be described within the same mathematical framework, which enables

the systematic synthesis and comparison of all feasible TMIA layouts. Note for the 1-AP TMIA, it is assumed to be installed at the mass element a_2 of the cable, exerting force F_{a_2} subjected to the mass velocity $\dot{x}_{a_2}$ and F_{a_1} shown in Fig. 1 is hence taken to be zero.

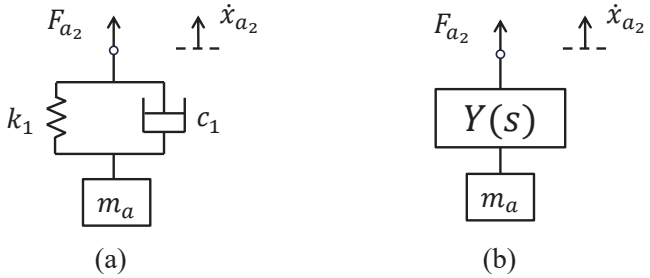

Figure 3: Absorbers with one attachment point: (a) the TMD and (b) the generic IF-network for TMIA

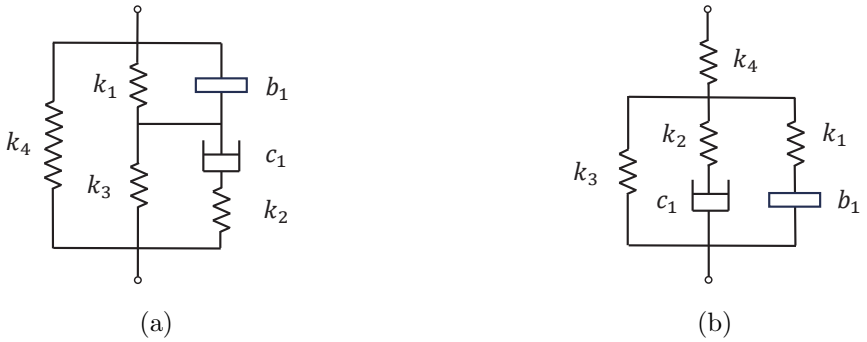

Figure 4: Networks (a) and (b) covering all layout possibilities consisting of one inerter, one damper, and one spring.

For the proposed generic IF-network of Fig. 3(b), the dynamic relationship between force F_{a_2} and velocity $\dot{x}_{a_2}$ can be derived in laplace domain as:

$$\tilde{F}_{a_2}(s) = \frac{Y(s) \cdot m_a s}{Y(s) + m_a s} \cdot \tilde{\dot{x}}_{a_2}(s) \tag{7}$$

where s represents the Laplace domain variable, and m_a denotes the reaction mass of the TMIA. Taking the TMD as an example, the relationship between its exerted force and the velocity can be represented by Eq. (7) with $Y(s)$ being $c_1 + k_1/s$. Consider the case that $Y(s)$ represents an inerter-based absorber comprising one spring, one damper, and one inerter. In this case, eight 1-AP TMIA layout possibilities can be formed from the generic IF network of Fig. 3(b) by considering all possible series–parallel interconnections with one of each type of two-terminal element, which are formulated using the structure-immittance approach [53]. With this approach, a full class of mechanical networks with a pre-determined number of inerters, dampers, and springs can be covered by a limited number of generic networks. For the present 1-AP TMIA case, one inerter, one damper, and one spring are considered for design simplicity. Following the formulation procedure in [53], the two generic networks shown in Fig. 4 (a) and (b) are obtained under the condition that only one physical spring is retained. The corresponding force–velocity transfer functions of these generic networks are then derived and

substituted into the $Y(s)$ block in Eq. (7), allowing all feasible 1-AP TMIA layouts to be explored systematically during optimisation. The transfer functions $Y(s)$ for the two generic networks are given as:

$$Y_1(s) = \frac{b_1 c_1 s^2 + b_1(k_3 + k_4)s + c_1(k_2 + k_3)}{b_1 c_1 (1/k_2)s^3 + b_1 s^2 + c_1 s + k_2 + k_3} \tag{8}$$

$$Y_2(s) = \frac{b_1 c_1 (1/k_1 + 1/k_2)s^3 + b_1 s^2 + c_1 s + k_3}{b_1(1/k_1 + 1/k_4)s^3 + c_1(1/k_2 + 1/k_4)s^2 + s} \tag{9}$$

with the conditions $b_1 \geq 0$, $c_1 \geq 0$,$k_i \geq 0$, and Eq. (8) requires that at least three of the four parameters k_1, $1/k_2$, k_3, k_4 are zero, corresponding to the left-side network in Fig. 4. Similarly, corresponding to the right-side network of Fig. 4, Eq. (9) requires at least three of the terms $1/k_1$, $1/k_2$,k_3 ,$1/k_4$ equal to 0. Based on these expressions of $Y(s)$, the TMIA exerted force F_{a_2} defined in Eq. (7), can then be adopted for further optimisation to identify the optimum TMIA configuration for cables.

3.2. 2-AP TMIA layouts

For the tuned mass inerter absorber featuring two structural attachment points, the most widely used configuration is the TMDI shown in Fig. 5(a), which has been extensively applied to various structures and has demonstrated significant vibration mitigation benefits. Nevertheless, numerous 2-AP TMIA possibilities remain unexplored, some of which may offer more advantageous dynamic characteristics. It should be noted that the TMIA configurations considered in this study employ the same set of physical components as the TMDI, namely one reaction mass, one spring, one damper, and one inerter, thereby ensuring a comparable level of implementation complexity. To systematically capture these possibilities, the method proposed in [52] is employed to enumerate all possible absorber layouts composed of a reaction mass and three two-terminal elements (one inerter, one damper and one spring). This leads to three generic IF networks, shown in Fig. 5(b-d).

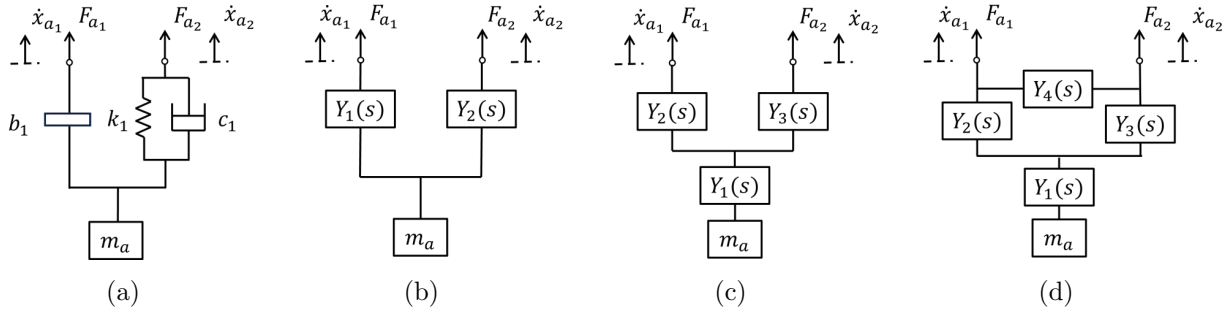

Figure 5: Tuned mass inerter absorbers with two attachment point: the TMDI (a) and the three generic IF-networks (b)(c)(d).

For the generic IF-network of Fig. 5(b), it can cover in total 16 absorber layouts by distributing all the three elements in one block and removing the other block. Here, block of Fig. 5(b) is removed means its transfer function $Y_1(s)$ or $Y_2(s)$ takes the value of infinity. To systematically analyse all the 16 network layouts, the transfer function of the present block including one each of the three element is formulated using the structure-immittance approach [53], which is shown as Eq. (8) and (9). Hence, for this generic IF-network, its generated

force F_{a_1}, F_{a_2} subjected to the cable velocity $\dot{x}_{a_1}$ and$\dot{x}_{a_2}$ can be derived in laplace domain as:

$$\begin{bmatrix} \tilde{F}_{a_1}(s) \\ \\ \tilde{F}_{a_2}(s) \end{bmatrix} = \frac{Y_1(s)Y_2(s)}{Y_1(s)+Y_2(s)+m_a s} \begin{bmatrix} \frac{Y_1(s)+m_a s}{Y_1(s)} & -1 \\ \\ -1 & \frac{Y_2(s)+m_a s}{Y_2(s)} \end{bmatrix} \begin{bmatrix} \tilde{\dot{x}}_{a_1}(s) \\ \\ \tilde{\dot{x}}_{a_2}(s) \end{bmatrix} \tag{10}$$

with the condition that one of the transfer function $Y_1(s)$, $Y_2(s)$, takes the expression of Eq. (8) or Eq. (9), and the other is infinity.

Considering the generic immittance-function network shown in Fig. 5(c), the potential absorber layouts are systematically generated by assigning the three two-terminal elements to two blocks, and the remaining block is excluded with its transfer function being infinity. Among the two retained blocks, one is allocated with a single element, and the other incorporates the remaining two, which can be connected in series or in parallel, forming two network possibilities. Since there are three different types of two-terminal elements involved, interchanging the positions of the present blocks will lead to different layouts, the IF-network of Fig. 5(c) can cover in total 36 TMIA layout possibilities. For instance, the TMDI can be formulated by distributing the parallel-connected spring-damper in block $Y_2(s)$, an inerter in $Y_3(s)$, and setting the transfer function of the remaining block $Y_1(s)$ to infinity. The force–velocity transfer function matrix for the IF-network of Fig. 5(c), in Laplace domain, can then written as:

$$\begin{bmatrix} \tilde{F}_{a_1}(s) \\ \\ \tilde{F}_{a_2}(s) \end{bmatrix} = \mathbf{L}(s) \begin{bmatrix} \tilde{\dot{x}}_{a_1}(s) \\ \\ \tilde{\dot{x}}_{a_2}(s) \end{bmatrix} \tag{11}$$

and

$$\mathbf{L}(s) = \frac{Y_2(s)Y_3(s)}{Y_2(s)+Y_3(s)+Y_m(s)} \begin{bmatrix} \frac{Y_2(s)+Y_m(s)}{Y_2(s)} & -1 \\ \\ -1 & \frac{Y_3(s)+Y_m(s)}{Y_3(s)} \end{bmatrix} \tag{12}$$

where $Y_m(s) = Y_1(s)m_a s/(Y_1(s)+m_a s)$ and one of the transfer functions $Y_1(s)$, $Y_2(s)$, $Y_3(s)$ must equal infinity, one represents a single element, and the left one corresponds to the networks involving the remaining two elements. These networks and the corresponding transfer functions can be formulated with the structure-immittance approach [53] for systematic analysis. In the scenario where $Y_2(s)$ represents an inerter b_1 and $Y_3(s)$ contains one spring k_1 and one damper c_1, the transfer functions of the IF-network are $Y_1(s) = \infty$, $Y_2(s) = b_1 s$, and $Y_3(s) = c_2(k_1/s + c_1)/(k_1/s + c_1 + c_2)$, covering all the potential networks for one damper and one spring under the condition that either c_1 or $1/c_2$ being zero.

For the generic IF-network shown in Fig. 5(d), three elements are distributed across three blocks, with the left block removed. In this case, for $Y_1(s)$, $Y_2(s)$ and $Y_3(s)$, its removal means the transfer function takes the value of infinity, while removing the block $Y_4(s)$ should make $Y_4(s) = 0$. Note that the layouts obtained by removing $Y_2(s)$ or $Y_3(s)$ will be reduced to that coverd by Fig. 5(c), hence are omitted in this case. As a result, a total of 12 TMIA layout possibilities can be enumerated with Fig. 5(d), and the generated forces of the two

attachment points can be derived as:

$$\begin{bmatrix} \tilde{F}_{a_1}(s) \\ \\ \tilde{F}_{a_2}(s) \end{bmatrix} = (\mathbf{L}(s) + Y_4(s)) \begin{bmatrix} 1 & -1 \\ \\ -1 & 1 \end{bmatrix} \begin{bmatrix} \tilde{\dot{x}}_{a_1}(s) \\ \\ \tilde{\dot{x}}_{a_2}(s) \end{bmatrix} \tag{13}$$

where either $Y_1(s) = \infty$ or $Y_4(s) = 0$ and each of the remaining three transfer functions represents a single two-terminal element, i.e. the damper, spring and inerter.

These obtained forces $\tilde{F}_{a_1}(s)$, $\tilde{F}_{a_2}(s)$ of the tuned mass inerter absorber with one or two attachment points shown in Eq. (7) and Eqs. (10-13) can then be substituted to the dynamic equations of the cable of Eq. (3), from which the damping ratio can subsequently be obtained and used for optimisation based on Eq. (5). The four generic IF-networks presented in this study enable the enumeration of a total of 72 possible TMIA layouts comprising a reaction mass, one spring, one damper, and one inerter. Instead of establishing and optimising these layouts as independent dynamic models, they are represented by the four generic immittance-function networks, each described by a corresponding transfer function. Using these generic IF-network representations together with the structure-immittance approach, all candidate TMIA layouts can be systematically analysed, and the optimum TMIA configuration can be identified through four optimisation problems. This representation significantly reduces the modelling effort and improves computational efficiency. For computational implementation, MATLAB is used throughout this work. A hybrid optimisation strategy is adopted, in which the derivative-free optimisation algorithm *patternsearch* is first used to explore the design space and identify promising candidate solutions, followed by *fminsearch* for local refinement. This strategy combines broad design-space exploration with efficient local optimisation, providing a practical balance between computational cost and solution accuracy. While alternative optimisation algorithms may also be suitable for this problem, the adopted hybrid strategy was found to be sufficiently efficient and robust for the present study. To reduce the possibility of convergence to local optima, multiple optimisation runs with different initial starting points were performed for each generic network, and repeated runs converged to the same optimum. In addition, the absorber parameters are nondimensionalized in this study for generality, where the nondimensional inertance b_1', damping coefficient c_1', stiffness k_1' and reaction mass m_a' are given as $b_1' = b_1/M$, $c_1' = (c'/M)/(\omega_0/\pi)$, $k_1' = (k_1/M)/(\omega_0/\pi)^2$, $m_a' = m_a/M$ and the absorber position relative to the total cable length, defined as a_i, are also presented in nondimensional forms as $a_i' = a_i/(n+1)$, with $i = 1, 2$ representing the two attachment point positions of the TMIA. The optimized parameters obtained in the following section are all provided in the nondimensional form.

4. Optimum results and performance verification

This section identifies the optimal absorber configurations for both single-attachment and two-attachment point layouts, using the generic immittance-function networks together with the structure-immittance approach. The robustness of the proposed absorbers is also assessed through sensitivity analysis, considering changes in absorber component values and installation positions. Note a single viscous damper and that with a TMD or a

Table 1: Optimization results and the corresponding parameter values

Types	Configurations	Damping ratio ζ_m	TMIA parameters			VD parameter c'
			Damping c_1'	Stiffness k_1'	Inertance b_1'	
Default	VD	0.0263	–	–	–	6.3753
1-AP	TMD	0.0939	0.0711	0.5273	–	4.6124
	$C1$	0.1165	0.0716	0.5266	0.5295	5.1442
2-AP	TMDI	0.2548	3.3526	5.3992	0.8567	6.3753
	$C2_1$	0.0273	4.1336	0.0615	1.4037	6.3280
	$C2_2$	0.2770	3.8252	1.1254	1.4367	6.3753
	$C2_3$	0.2883	3.9302	1.1510	1.3706	6.3753

TMDI are also optimized for the sake of comparison.

4.1. Identification of optimum absorber configurations

Consider the cable model with absorbers shown in Fig. 1, the damper is mounted in a fixed position, 5% along the span of the cable. For the TMIA with one attachment point, the absorber is placed at 20% length from one end of the cable, i.e. $a_2' = 0.2$, and for the TMIA with two attachment points, one point is attached to the position as $a_1' = 0.1$, and the other attachment point is also placed to the cable with $a_2' = 0.2$. Note that the absorber can be installed in other positions, and here we select the above position as an example to explore the potential benefits of applying the proposed method for absorber design.

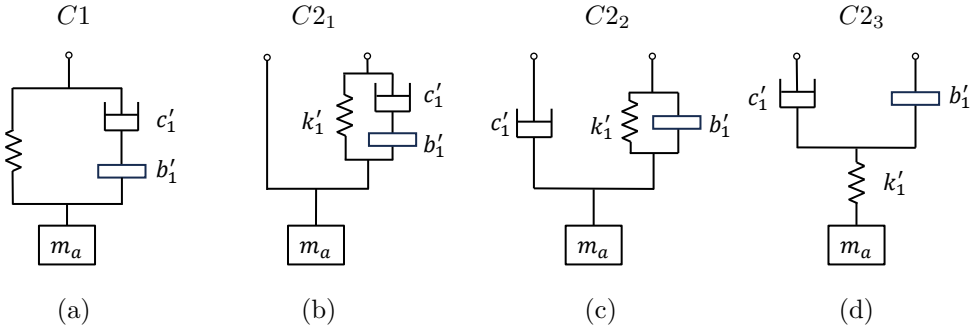

Figure 6: Optimum configurations for the TMIA with one attachment point (a)$C1$, and two attachment points (b) $C2_1$, (c)$C2_2$ and (d) $C2_3$.

The optimization problem expressed in Eq. (5) is now used, and the added reaction mass m_a is taken as 5% of the total cable mass, i.e. $m_a' = 0.05$, which is in line with [64] for using the TMD to suppress the cable vibration. The cable model with VD only is also optimized, suggesting that with a single viscous damper, the minimum damping ratio ζ_m of 0.0263 is achieved around the first mode when the non-dimensional damping coefficient c' is set to be 6.375. To ensure the required damping value c' is no larger than the default one, the damping coefficient of the viscous damper is limited as $c' \leq 6.375$ during the optimisation process. The optimization results, together with the obtained absorber configurations are shown in Table 1 and Fig. 6, respectively. It should be noted that Fig. 6(a) represents the optimal 1-AP TMIA configuration, denoted as $C1$, obtained from the generic IF-network shown in Fig. 3. Fig. 6(b)–(d) represent the optimal 2-AP TMIA configurations,

Table 2: 2nd to 4th modes damping ratio

Mode	VD	TMD	$C1$	TMDI	$C2_3$
2	0.0206	0.0366	0.0352	0.1004	0.0830
3	0.0148	0.0288	0.0272	0.0546	0.0571
4	0.0111	0.0208	0.0194	0.0152	0.0225

denoted as $C2_1$, $C2_2$, and $C2_3$, which are obtained from the three generic IF-networks shown in Fig. 5(b)–(d), respectively. To obtain the optimum results reported above, a complete optimisation run with a single set of initial values requires approximately 285 min in total. The reported computational time was obtained using MATLAB on a standard desktop computer equipped with an Intel Core i7 processor and 32.0 GB RAM, with the optimisation performed on a single core. To reduce the possibility of convergence to local optima, multiple optimisation runs with different initial starting points were also conducted. The repeated runs converged to the same optimum, indicating satisfactory convergence repeatability for the present optimisation problem. It should also be noted that the optimisation of different generic networks and the multi-start optimisation runs are independent of each other. Therefore, the computational time could be further reduced by using parallel computing, multi-core implementation, or more efficient global optimisation strategies. The TMD and TMDI, which are widely used as benchmark 1-AP and 2-AP absorber systems, respectively, are also optimised for comparison.

For the optimum 1-AP TMIA configuration, $C1$ shown in Fig. 6(a), the minimum damping ratio is increased from 0.0939 for the classical TMD to 0.1165, corresponding to an improvement of approximately 24.1%. This improvement is achieved with only limited additional implementation complexity compared with the classical TMD. Considering the optimum 2-AP TMIA absorbers, $C2_1$, $C2_2$ and $C2_3$ shown in Fig. 5, the $C2_1$ provides ignorable better performance than a default viscous damper, this is because the reaction mass m_a is directly attached to the cable and the relative movement between the absorber's two terminals is relatively small, resulting in limited vibration suppression performance. The TMDI configuration is encompassed within the generic IF network of Fig. 5(b), while the optimum absorber is $C2_2$, shown in Fig. 6(c), with which the value of ζ_m is obtained as 0.277. Compared with the TMDI, $C2_2$ can result in 8% performance improvement. $C2_3$, the optimum configuration obtained from the generic IF-network of Fig. 5(d), is the most effective absorber among all the 72 layouts possibilities consisting of one reaction mass, one damper, one inerter and one spring. From Table 1, it can be noted that $C2_3$ outperforms $C1$ with 147% performance improvement in ζ_m, suggesting that the absorber with two attachment points can provide better vibration suppression performance than that of one attachment point containing an equal quantity of each component type. It can also be noted that $C2_3$ outperforms the conventional TMDI, providing a 13.1% improvement in the damping ratio. The superior performance of $C2_3$ can be attributed to its distinct interconnection topology. Compared with the conventional TMDI, the spring is located between the reaction mass and the intermediate node connecting the inerter and damper, introducing additional flexibility into the absorber subsystem. This modified dynamic coupling alters the interaction among the absorber components and allows a more effective utilisation of the inerter and damper

effects. As a result, a higher attainable damping ratio can be achieved within the target frequency range. In addition, the damping ratio of other three modes of the cable model are also analyzed and summarized in Table 2, suggesting that the obtained configurations will not deteriorate the damping ratio of higher modes within $\omega_i \in (1.5\omega_0 - 4.5\omega_0)$.

4.2. Parametric sensitivity analysis

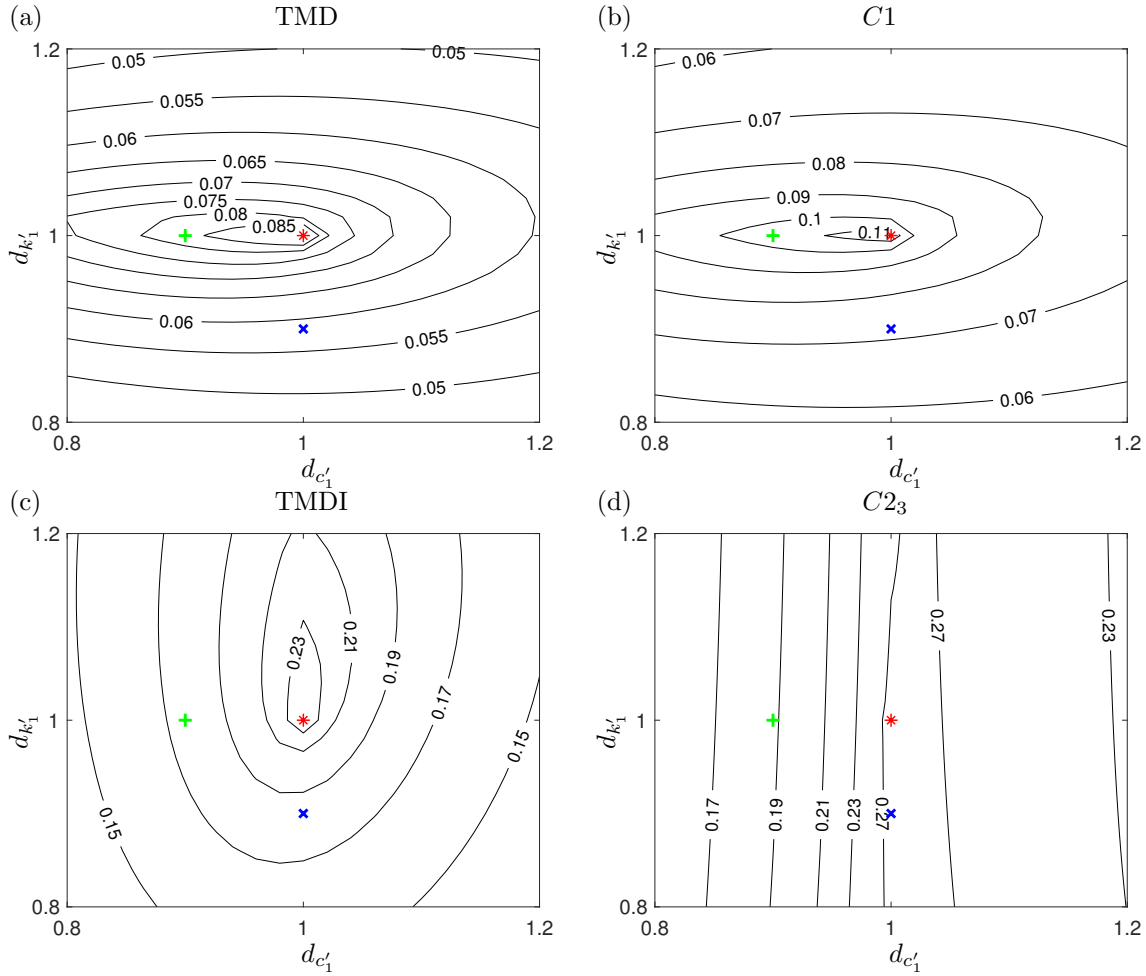

Figure 7: Minimum damping ratio ζ_m with respect to the deviation of stiffness k_1' and damping c_1' for the absorbers: (a) TMD, (b) $C1$, (c) TMDI and (d) $C2_3$.

In the previous research, the TMIA parameters were determined as specific values by optimisation approaches. However, the parameters may have deviations in practical engineering due to installation error and component wearing, which may deteriorate the vibration suppression effectiveness of the system. Therefore, it is essential to evaluate the robustness of the absorbers versus the parameter changes. For the analysis, absorber parameters are varied between ±20% of the default values provided in Table 1. The deviation rate of parameters is defined as a deviation factor d within the range of [0.8, 1.2]. In the sensitivity analysis, the optimal configuration for the 1-AP TMIA ($C1$) and the 2-AP TMIA ($C2_3$) are considered. The performance of traditional absorbers, the TMD and the TMDI are also considered for comparison. Fig. 7 presents the contour plot of the

minimum damping ratio ζ_m from Eq. (5), with respect to the absorber stiffness k_1' and damping c_1'.

The optimum damping ratio ζ_m and the corresponding parameter values are marked as red asterisks in Fig. 7, where the blue cross symbol indicates the performance for $d_{k_1'} = 0.9$ and green plus sign shows performance for $d_{c_1'} = 0.9$. From Fig. 7, it is evident that the performance measure ζ_m is more sensitive to the changes of absorber stiffness k_1' for the 1-AP TMIA ($C1$) and the TMD, while the 2-AP TMIA ($C2_3$) and the TMDI are more sensitive to the damping variations. For the case that the absorber damping varies to 90% of the default value, i.e. $d_{c_1'} = 0.9$ and all other parameters are maintained at their default values (as indicated by the green plus sign), the value of ζ_m for the TMD and the $C1$ can be obtained as 0.079 and 0.103, approximately 15.1% and 11.2% lower than their respective optimum values. It can also noted from Fig. 7(a) and (b) that $C1$ consistently provides higher damping performance than the TMD within the considered ranges of stiffness and damping deviations. For the 2-AP TMIA, the TMDI and the optimum configuration $C2_3$, the minimum damping ratio ζ_m is respectively decreased to 0.175 and 0.188. It can be seen that the $C2_3$ can still provide performance benefits than the TMDI, approximately 7.4% larger value of ζ_m. Consider the case that the absorber stiffness varies by -10% of the default value, i.e. $d_{k_1'} = 0.9$ (shown as blue cross sign in Fig. 7), the minimum damping ratio ζ_m of the TMDI and the $C2_3$ is decreased by 27.3% and 4.5% of the default optimum value, to 0.185 and 0.272. While for the absorber with one attachment point, the value of ζ_m is changed to 0.058 for the TMD and 0.072 for the $C1$, significantly smaller than that of the $C2_3$. From Fig. 7, it can also be noted that the proposed optimum TMIA $C2_3$ is most robust to the absorber stiffness k_1', and provides the best vibration mitigation performance compared to the other absorbers, in the whole range of absorber stiffness and damping values.

Considering that cable tension may be affected by temperature variations and long-term service conditions, the robustness of the proposed absorbers against cable tension variation is also investigated. Since cable tension directly affects the cable stiffness, its influence is represented by varying the cable stiffness (k) by $\pm 20\%$ from the nominal value. Fig. 8(a) plots the minimum damping ratio ζ_m for the different absorbers, i.e., TMD, TMDI, $C1$, and $C2_3$, as a function of the cable stiffness variation ratio d_k. It is observed that $C2_3$ consistently maintains the highest minimum damping ratio among all considered absorbers throughout the investigated range. This demonstrates that $C2_3$ retains its superior vibration suppression capability under the considered cable stiffness variations. In addition, the influence of reaction-mass variation is examined, as shown in Fig. 8(b). In this analysis, the reaction mass is varied from -20% to +20% relative to its nominal value, while the other optimised absorber parameters are kept unchanged. The results show that $C2_3$ maintains the highest minimum damping ratio among all considered absorbers throughout this moderate mass-variation range. Notably, when the reaction mass is reduced by 20%, i.e., $m_a' = 0.04$, $C2_3$ still achieves $\zeta_m = 0.251$, indicating that its performance degradation under moderate reaction-mass reduction is limited. However, the performance gap between $C2_3$ and TMDI becomes smaller as the reaction mass decreases. To further examine lower reaction-mass conditions, additional cases with $m_a' = 0.03$ and $m_a' = 0.02$ were also considered. The results are summarized in Table 3. It should be noted that these additional cases are also evaluated using the absorber parameters optimised at the nominal mass ratio, without re-optimisation for the reduced mass ratios. The results show

that under these substantially reduced mass ratios, the performance advantage of the nominally optimised $C2_3$ becomes less pronounced, and the conventional TMDI can provide a higher minimum damping ratio. This suggests that $C2_3$, when optimised at the nominal mass ratio, may become less favourable under very low reaction-mass conditions. Therefore, when a substantially lower reaction mass is imposed, the absorber parameters and possibly the topology need to be re-optimised.

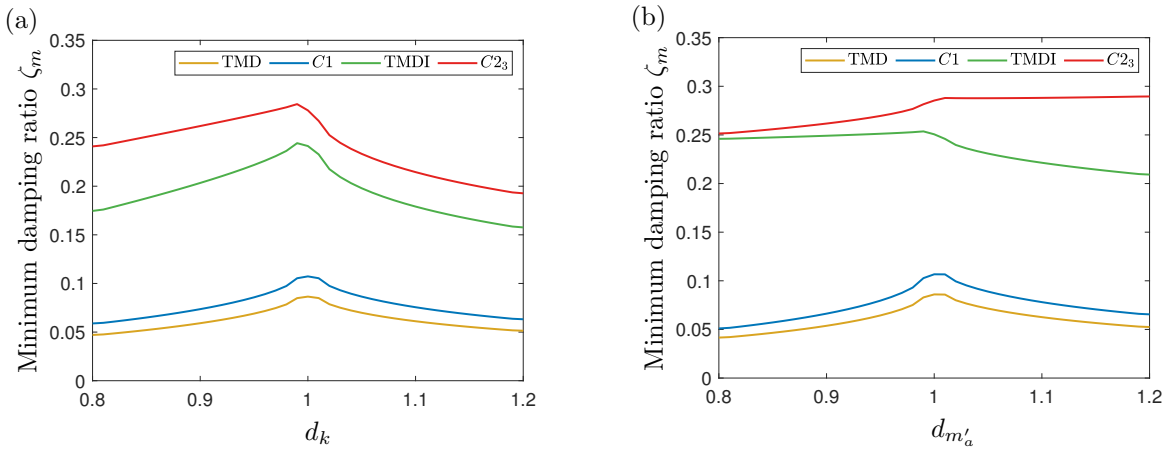

Figure 8: Minimum damping ratio ζ_m with respect to the deviation of (a) cable stiffness k and (b) reaction mass m'_a

Table 3: Minimum damping ratio for the selected smaller mass ratio.

mass ratio m'_a	minimum damping ratio ζ_m			
	TMD	$C1$	TMDI	$C2_3$
0.03	0.029	0.035	0.241	0.237
0.02	0.024	0.029	0.236	0.228

Effects of absorber location on the cable performance are also considered in this work, where for the absorber with two attachment points, one terminal is fixed at the position of $a'_1 = 0.1$ and the other terminal is attached to different positions. The absorber's location is represented by a'_2 within the range of [0.2,0.5]. Note that in this analysis, the parameter values of absorber are kept unchanged, and the performance measure, the minimum damping ratio ζ_m with various absorber locations are shown in Fig. 9. It can be seen that the value of ζ_m of all the considered absorbers decreases with the installation position a'_2 increasing, which means a worse vibration mitigation performance. The optimum one attachment point TMIA, the $C1$, provides similar performance of the TMD for all the installation positions. Consider the absorbers with two attachment points, the $C2_3$ has the minimal reduction rate, which indicates a superior robustness to the absorber location. In addition, it can be noticed that the $C2_3$ can provide the best damping enhancement performance amongst all the absorbers in the whole position range.

4.3. Numerical Verification

This section demonstrates the performance improvements of the proposed absorbers by subjecting the cable model to earthquake excitations and wind loads. Specifically, three earthquake ground motions are considered,

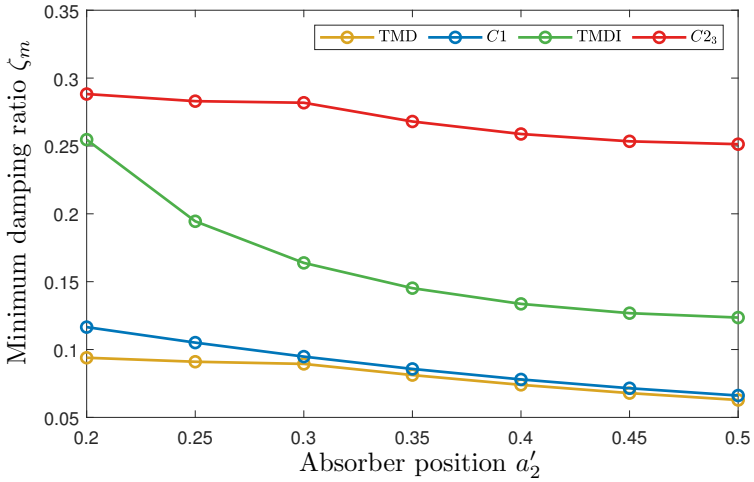

Figure 9: Minimum damping ratio ζ_m with respect to the changes of absorber location.

while the wind loads are simulated based on the Kaimal spectrum for the along-wind direction.

4.3.1. Earthquake excitation

To illustrate the effectiveness of the proposed TMIAs with one or two attachment points in cable vibration suppression, i.e. TMD, $C1$, TMDI and $C2_3$, the established cable model is firstly subjected to the earthquake excitations. The cable parameters are taken from [4], listed in Table 4. Three earthquake records, namely the El-Centro, Tohoku, and Kobe records, are adopted in the analysis, with their detailed information summarized in Table 5. These records are selected to represent different seismic characteristics. Specifically, the El-Centro record is a widely used benchmark ground motion with pronounced low-frequency content, the Tohoku record represents a large-magnitude long-duration subduction earthquake with broadband frequency content, and the Kobe record represents a near-field high-PGA earthquake with impulsive characteristics, thereby enabling the proposed TMIA configurations to be evaluated under different seismic inputs. Earthquake excitations are applied to the 1st and the nth mass elements of the cable model shown in Fig. 1. The mid span displacement ($x_{(n+1)/2}$) is considered as the performance measure, for which the root mean square and maximum values (RMS($x_{(n+1)/2}$) and MAX($x_{(n+1)/2}$)) are calculated and summarized in Table 6.

Table 4: Parameters of the cable model

Length L(m)	Mass m(kg/m)	Diameter D(m)	Tension T(kN)	Angle $\theta(^\circ)$	deck height z_0(m)
334.2	64.5	0.128	4182.5	34	72

As shown in Table 6, all the four absorbers notably enhance the cable's vibration suppression performance compared to the default response with only a viscous damper installed. For the TMIA with one attachment point, the midspan response $x_{(n+1)/2}$ of the $C1$ is similar to that of the TMD, showing slightly performance benefits. The traditional absorbers with two attachment points, i.e. the TMDI, can strengthen the vibration alleviating performance, reducing at most 38.7% and 27.4% smaller value of RMS($x_{(n+1)/2}$) and MAX($x_{(n+1)/2}$) compared to the TMD for all the three earthquakes. In addition, the optimum TMIA with two attachment

Table 5: Information of Earthquake excitations.

Earthquake	Station	Year	Magnitude (Mw)	PG (g)	Component
El-Centro	Imperial Valley Irrigation District	1940	6.9	0.348	NS
Tohoku	Fukushima (MYG004)	2011	9.0	0.270	NS
Kobe	Kobe University (JMA)	1995	6.9	0.821	NS

Table 6: Root mean square and maximum values of cable midspan displacement under earthquake excitations.

Earthquake type	$x_{(n+1)/2}$ $\times 10^{-3}$ m	Absorber configurations				
		VD	TMD	$C1$	TMDI	$C2_3$
Tohoku	RMS	5.27	3.80 (27.9%/−)	3.76 (28.7%/1.1%)	2.50 (52.6%/34.2%)	2.36 (55.2%/37.9%)
	MAX	19.8	17.5 (11.6%/−)	17.4 (12.1%/0.6%)	12.7 (35.9%/27.4%)	11.7 (40.9%/33.1%)
Kobe	RMS	5.20	4.50 (13.5%/−)	4.48 (13.8%/0.4%)	3.91 (24.8%/13.1%)	3.70 (28.8%/17.8%)
	MAX	32.9	31.3 (4.9%/−)	31.2 (5.2%/0.3%)	28.3 (14.0%/9.6%)	26.2 (20.4%/16.3%)
El-centro	RMS	8.11	6.49 (20.0%/−)	6.32 (22.1%/2.6%)	3.98 (50.9%/38.7%)	3.69 (54.5%/43.1%)
	MAX	23.2	21.6 (6.9%/−)	21.4 (7.8%/0.9%)	16.0 (31.0%/25.9%)	14.9 (35.8%/31.0%)

points, the $C2_3$, outperforms the other three absorbers, and comparing with the TMDI, the $C2_3$ can further reduce the RMS and maximum midspan displacement by at most 7.3% and 7.9% under all the earthquake types. Table 7 shows the maximum stroke of the considered absorbers, i.e. the TMD, the C1, the TMDI and the $C2_3$, suggesting that the $C1$ and the TMD have similar mass displacement, and although the TMDI can provide better vibration mitigation performance, its stroke is significantly larger than that of the TMD. For the optimum 2-AP TMIA, the $C2_3$, its stroke is even smaller than that of the TMD, further illustrating the vibration suppression superority of the proposed absorber.

Taking the EI-centro earthquake shown in Fig. 10(a) as an example, Fig. 10(b) shows the midspan displacement, $x_{(n+1)/2}$, of the cable subjected to this excitation. The PSD of the $x_{(n+1)/2}$ is plotted in Fig. 10(c), which is achieved using MATLAB Pwelch function with flat top weighted window. For the traditional viscous damper, the maximum PSD value of $x_{(n+1)/2}$ is 0.0148m^2/Hz, which can be significantly suppressed by adding an additional absorber, for example, with an additional TMD, the PSD value of $x_{(n+1)/2}$ can be reduced to 0.0118m^2/Hz, approximately 20.3% smaller than that of the VD. The optimum 1-AP TMIA, the C1, provides slightly smaller response of midspan displacement for the EI-centro earthquake. Consider the 2-AP absorbers, the maximum PSD values of $x_{(n+1)/2}$ for the TMDI and the $C2_3$ are respectively 0.0064m^2/Hz and 0.0059m^2/Hz, providing 45.7% and 50.0% performance improvement compared to the TMD. The corresponding

Table 7: Maximum absorber stroke subjected to earthquake excitations.

Earthquake type	Maximum absorber stroke $\times 10^{-3}$ m			
	TMD	$C1$	TMDI	$C2_3$
Tohoku	24.1	23.6	102.0	7.5
Kobe	23.0	22.7	114.3	10.2
El-centro	24.7	24.0	96.7	7.4

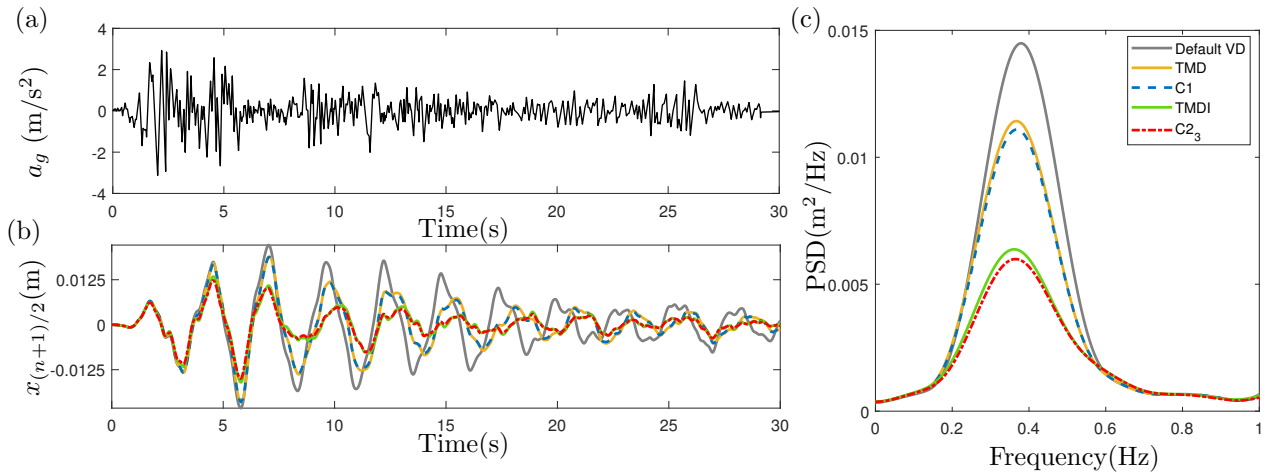

Figure 10: Midspan displacement of the cable subjected to the EI-centro earthquake (a) in time domain (b) and frequency domain (c).

midspan displacement responses in time domain are plotted in Fig. 10(b), where the maximum displacement of the $C2_3$ is 0.0149m, approximately 31% and 6.9% smaller than that of the TMD and the TMDI. In terms of the root mean square value of $x_{(n+1)/2}$, the $C2_3$ also outperforms the other absorbers, as illustrated in Table 6. These obtained results suggest that the optimum TMIA with two attachment points, the $C2_3$ can significantly enhance the vibration suppression performance of the cable under earthquake excitations compared to the existing absorbers, demonstrating the effectiveness of the design methodology proposed for tuned mass inerter absorbers.

4.3.2. Wind excitation

In this subsection, the effectiveness of the proposed absorbers in mitigating cable vibrations is further validated under wind loads, for which the along wind speed is expressed by[65]:

$$U_i(z_i,t) = \bar{U}_i(z_i) + u(z_i,t) \tag{14}$$

where $\bar{U}_i(z_i)$ denotes the mean wind velocity, $u(z_i,t)$ is the wind velocity fluctuations and z_i is the vertical coordinate of the ith mass element. By assuming that the wind speed and height of the bridge deck are $\bar{U}_0$ and z_0, for the ith element of the FEM cable model, the mean wind speed can be written as:

$$\bar{U}_i = \bar{U}_0(\frac{z_i}{z_0})^{\alpha} \tag{15}$$

and

$$z_i = \frac{iL}{n+1} \cdot \sin\theta + z_0 \tag{16}$$

where θ is the cable inclination angle, α is dimensionless exponent, selected as 0.12 which is in line with [66]. The wind velocity fluctuations $u(z_i, t)$ is generated based on the Kaimal spectrum, simulated by:

$$\frac{\omega_u S_u(z_i, \omega_u)}{u_*^2} = \frac{200f}{(1+50f)^{5/3}} \tag{17}$$

and

$$f = \frac{\omega_u z_i}{\bar{U}_i} \tag{18}$$

with ω_u being the wind velocity frequency, u_* being the friction velocity of wind and f representing the Monin coordinates.

Based on the Eqs. 14-18, time histories of the wind velocity $U_i(z_i, t)$ can be generated using the discrete frequency function in conjunction with the Fast Fourier Transform method. Following field test data of Sutong Bridge[66], the wind friction speed is taken as $u_* = 0.7394$, and by setting the mean wind velocity at the bridge deck U_0 as 13.97m/s, the time domain wind velocity of any mass element of the cable can be obtained. For instance, Fig. 11(a) shows the wind velocity of the mass element located at $0.1L$, $0.5L$, and $0.9L$ of the cable, where the wind velocity at the position of $0.1L$ is also shown in frequency domain as an example, see Fig. 11(b). With the obtained wind velocity, the wind force acting on the ith element of the cable model can subsequently be obtained by:

$$F_{wind}(z_i, t) = \frac{1}{2}\rho C_D D \cdot \frac{L}{n+1} \cdot U_i^2(z_i, t) sin^2\theta \tag{19}$$

where ρ is air density, D is the diameter of cable, C_D is the drag coefficient.

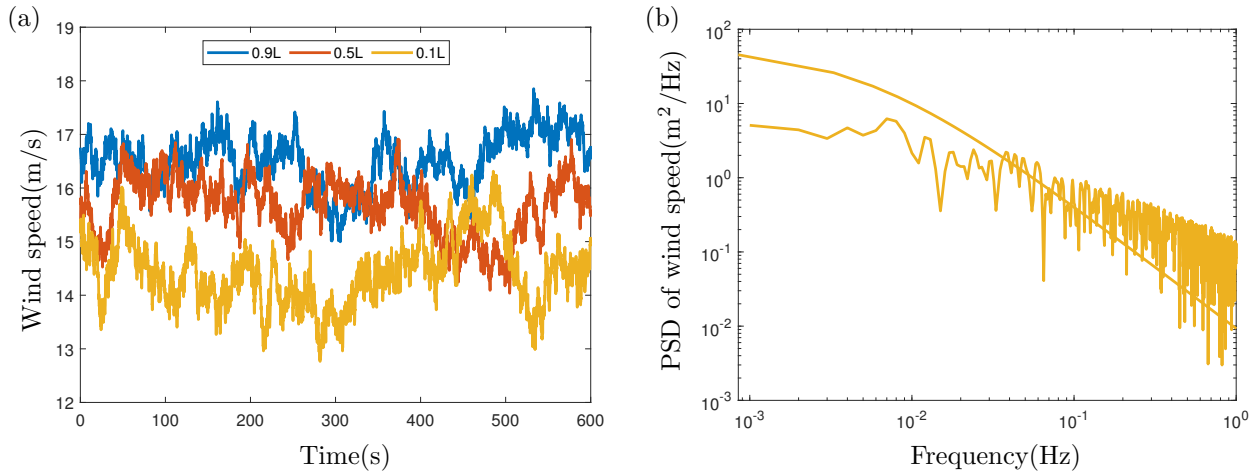

Figure 11: The time domain wind speed on the cable location of 0.9L(blue), 0.5L(red), 0.1L(yellow) (a) and the corresponding PSD of an example loacation, i.e.0.1L.

For the load case with the mean wind velocity $U_0 = 13.97$m/s, the dynamic responses of midspan displacement, $x_{(n+1)/2}$, with the proposed absorbers subjected to the wind forces can hence be simulated, shown as Fig. 12(a) in time domain and Fig. 12(c) in frequency domain. Fig. 12(b) shows the time domain response of the cable midspan in a narrowed time window. The default response with a single VD is also presented in Fig. 12 for the sake of comparison. Table 8 summarizes the RMS and peak value of the time domain midspan

displacement of the cable, as well as the corresponding Power Spectral Density (PSD) in the frequency range of [0.2Hz, 0.8Hz]. Fig. 12(c) shows that the $C1$ has similar performance with the TMD, providing approximately 53% performance improvement in the maximum amplitude around 0.38Hz compared to the default system with a single VD. It is also noted that the tuned mass inerter absorbers with two attachment points, i.e. the TMDI and the optimum $C2_3$ have better vibration suppression performance than the 1-AP TMIA, resulting in 60.5% and 69.3% smaller values of the maximum PSD. For the root mean square value of the PSD, the TMDI can reduce the response by 52.1% compared to the TMD, and the $C2_3$ can further reduce the RMS of the PSD by 59.3%. The maximum value of the time domian midspan dispacement of the cable with a VD is 5.74 mm, which is slightly larger than that with an additional TMD and the $C1$. The TMDI can mitigate the maximum displacement to 5.42 mm, with 5% performance improvement than the TMD. The optimum TMIA, the $C2_3$ outperforms the other absorbers, providing 8.8% and 4.2% smaller value of MAX($x_{(n+1)/2}$) compared to the TMD and the TMDI. It can also be noted from Table 8 that the $C2_3$ is also superior in RMS value of $x_{(n+1)/2}$. Furthermore, the stroke of the considered absorbers under wind loads is also studied, and the results suggest that the maximum stroke of the optimum 1-AP absorbers, the C1, is slightly smaller than that of the TMD, and the $C2_3$ results in the maximum stroke as 3.5mm, which is smallest among all the considered absorbers, approximately 87.6% smaller than the TMDI.

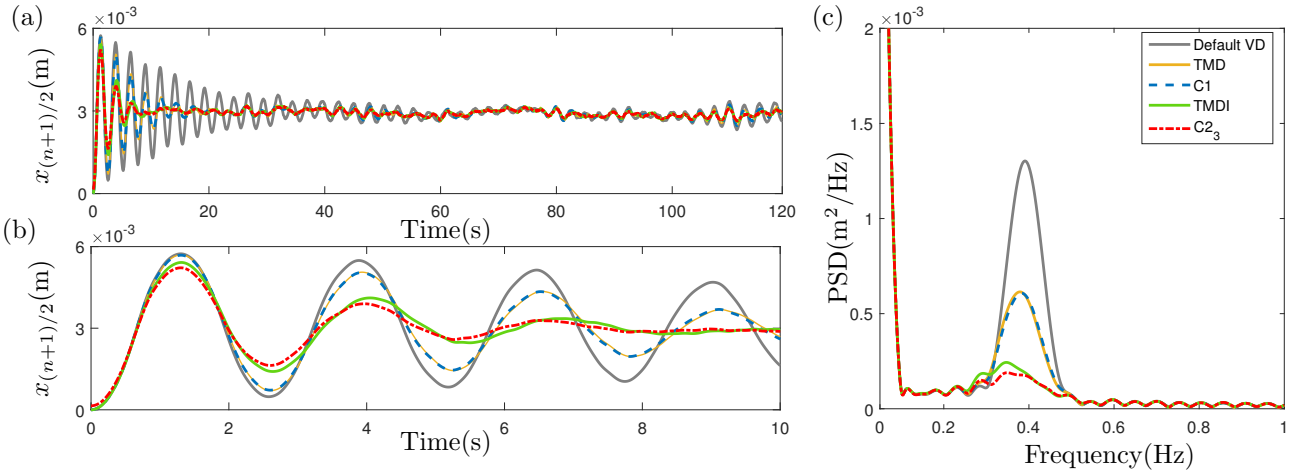

Figure 12: Midspan displacement of the cable subjected to the wind loads in (a) time domain, (b) a narrowed time window and (c) frequency domain.

Table 8: Midspan response of the cable subjected to the wind loads

Performance	VD	TMD	$C1$	TMDI	$C2_3$
MAX $x_{(n+1)/2}$ ($\times 10^{-3}$m)	5.74	5.70 (0.7%/−)	5.68 (1.0%/0.4%)	5.42 (5.6%/5.0%)	5.20 (9.4%/8.8%)
RMS $x_{(n+1)/2}$ ($\times 10^{-3}$m)	3.01	2.97 (1.3%/−)	2.97 (1.3%/−)	2.94 (2.3%/1.0%)	2.91 (3.3%/2.1%)
MAX PSD ($\times 10^{-4}$m^2/Hz)	13.0	6.15 (52.7%/−)	6.07 (53.3%/1.3%)	2.43 (81.3%/60.5%)	1.89 (85.5%/69.3%)
RMS PSD ($\times 10^{-4}$m^2/Hz)	4.56	2.36 (48.2%/−)	2.33 (48.9%/1.3%)	1.13 (75.2%/52.1%)	0.96 (78.9%/59.3%)

Taken together, the above results further demonstrate the engineering applicability of the proposed TMIA configurations. Compared with the conventional TMD, the optimal configuration $C2_3$ provides substantial vi-

Table 9: Maximum absorber stroke subjected to wind excitations.

Excitation type	Maximum absorber stroke $\times 10^{-3}$ m			
	TMD	$C1$	TMDI	$C2_3$
wind	8.93	7.68	28.4	3.51

bration mitigation improvement under both earthquake and wind excitations. Although the response reduction achieved by $C2_3$ relative to the conventional TMDI is more modest, $C2_3$ requires a much smaller maximum absorber stroke under the considered loading cases, as shown in Tables 7 and 9. This indicates that the proposed configuration offers a favourable trade-off between vibration mitigation performance and implementation requirements. The superior performance of $C2_3$ is also consistently observed under earthquake records with different characteristics as well as under stochastic wind excitation, demonstrating satisfactory robustness with respect to loading conditions. While only a representative stochastic wind field is considered in the present study, the influence of different wind characteristics on TMIA performance warrants further investigation.

5. Design refinement with experimentally verified parasitic effects

The optimal configuration $C2_3$ can be physically realised using two cable attachment points connected through a spring, a damper, an inerter, and a reaction mass. The spring, damper, and reaction mass are conventional mechanical components that can be implemented using technologies similar to those adopted in existing TMD and TMDI systems [67, 68]. As the inerter represents the most challenging element for practical realisation, this study focuses exclusively on its nonlinear characteristics. The parameters of the optimal configuration $C2_3$ are then refined to maintain the vibration suppression performance. Finally, the performance of the refined design is verified under earthquake and wind excitations.

5.1. Parasitic effects identification

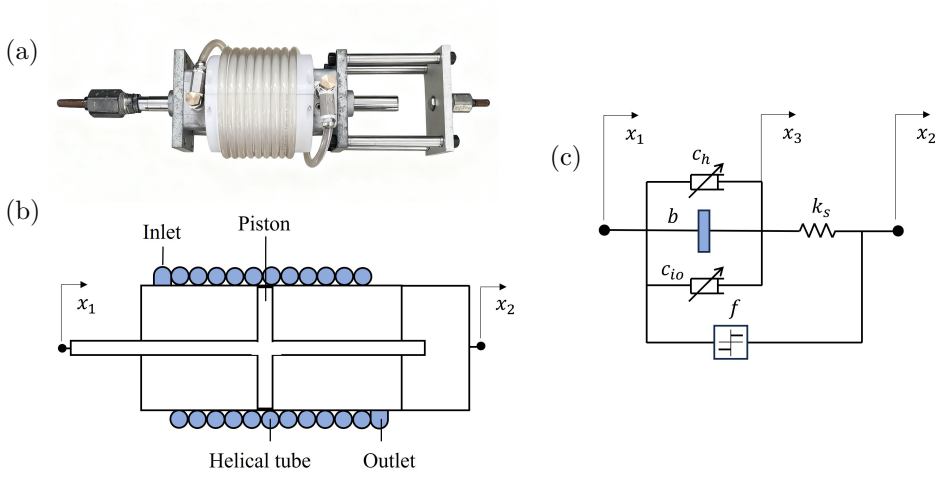

Figure 13: Prototype (a), schematic (b) and mechanical (c) model of a fluid inerter

The physical realisation of the inerter is schematically shown in Fig. 13(a),(b), known as the fluid inerter with the advantages of improved durability, inherent damping and simplicity of design. The corresponding mechanical model is also provided in Fig. 13(c). The inertance of the fluid inerter is formed by the fluid passing through the helical tube due to the movement between the piston and the cylinder, derived as

$$b = \rho l \frac{{A_1}^2}{A_2} \tag{20}$$

where ρ is the fluid density, l is the helical tube length, A_1 is the piston area and A_2 is the tube area. In addition to the inertance, the fluid inerter has parasitic effects due to the prototype design, these are the helical tube damping c_h, the inlet-outlet damping c_{io}, the effective stiffness k_s and the friction f. The helical tube damping is caused by the viscous effects in the helical tube, which can be expressed as

$$c_h = f_c \frac{2\rho l A_1^3}{D_h A_2^2}(\dot{x}_3 - \dot{x}_1) \tag{21}$$

with f_c being the Fanning friction factor, equal to

$$f_c = 0.08 Re^{-1/4} + 0.012\sqrt{\frac{D_h}{2R}} \tag{22}$$

where $Re = \rho D_h A_1(\dot{x}_3 - \dot{x}_1)/(\mu A_2)$ is the Reynolds number of the helical tube flow, D_h is the tube diameter, R is the helix radius and μ is the fluid viscosity at reference temperature. In addition to c_h, the other damping effects of the fluid inerter occur at either end of the fluid channel (inlet and outlet), formulated as

$$c_{io} = 0.75 \frac{\rho A_1^3}{A_2^2}(\dot{x}_3 - \dot{x}_1) \tag{23}$$

The effective stiffness k_s of the fluid inerter is mainly caused by the fluid compressibility and the air dissolved in the fluid, which is identified by matching the theoretical model with the experimental results, and the friction f is also captured experimentally. In this study, a fluid inerter prototype with the parameters listed in Table 10 is built and tested shown in Fig. 14(a), where the friction force is firstly identified by selecting the 10mm displacement triangle wave with 0.01Hz frequency as the excitation input (see Fig. 14(b)). It can be seen from Fig. 14(c), the friction of this prototype is approximately 40N. To capture the effective stiffness, sinusoidal displacements with 5mm amplitude and various frequencies in the range of [0Hz, 5Hz] are selected as the excitation input. Note that the frequency range is selected based on the vibration frequency of the stay cable, which is normally between 0.25Hz and 5Hz. The force exerted by the inerter can then be recorded via experiment, and the correlation method [69] is applied to achieve the force to velocity transfer function of the device at each tested frequency. The magnitude and phase of the calculated transfer function are shown as red cross marks in Fig. 15, which are subsequently used to identify the effective stiffness k_s by matching the theoretical results with the experimental ones. A metric H is introduced to quantify the root mean square

Table 10: Parameters of the fluid inerter prototype.

Description	Value
Area of piston A_1 (m^2)	4.5×10^{-3}
Area of tube A_2 (m^2)	5×10^{-5}
Helix radius R (m)	0.081
Length of helical tube l (m)	5.19
Diameter of tube D_h (m)	0.008
Density of working fluid ρ at 30°C ($kg \cdot m^{-3}$)	995.6
Viscosity of working fluid μ at 30°C (Pa·s)	7.98×10^{-4}

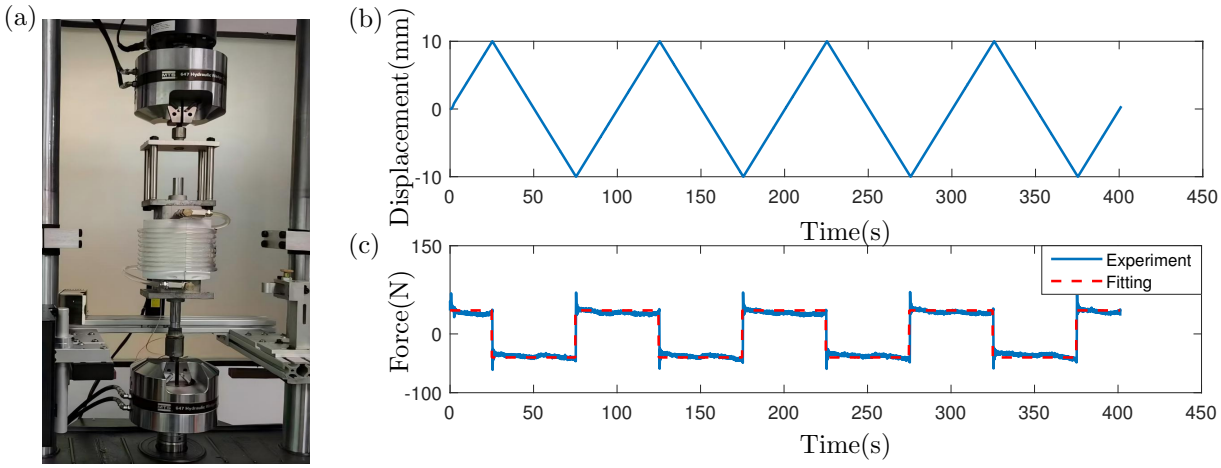

Figure 14: Experiment setup (a), displacement input (b) and the exerted force (c) of the fluid inerter.

discrepancy between experimental and theoretical results, as

$$H = \frac{1}{N}\sqrt{\sum_{i=1}^{N} |T(k_s, j\omega_i) - E(j\omega_i)|^2}$$

where N is the number of frequencies, $T(k_s, j\omega_i)$ and $E(j\omega_i)$ are the admittance function obtained based on the numerical simulation and experimental test. By minimising the value of H, the effective stiffness can hence be obtained as $k_s = 815.6$kN, with which the theoretical results are shown as solid lines in Fig. 15. Very good agreement can be noticed. The force-time histories and hysteretic loops of the fluid inerter are also checked to illustrate the validity of the theoretical model, and Fig. 16 shows the theoretical and experimental inerter forces at frequencies of 0.75 Hz and 2 Hz, suggesting that the mechanical model in Fig. 13, with the identified parasitic effects, can accurately predict the characteristics of the fluid inerter.

5.2. Design refinement

In Section 4, a significant performance improvement in vibration suppression of the cable model has been achieved with the proposed 2-AP TMIA configuration, the $C2_3$. However, the absorber components are assumed to be ideal, i.e. no parasitic effects associated with physical realisation are considered. To check the impact of

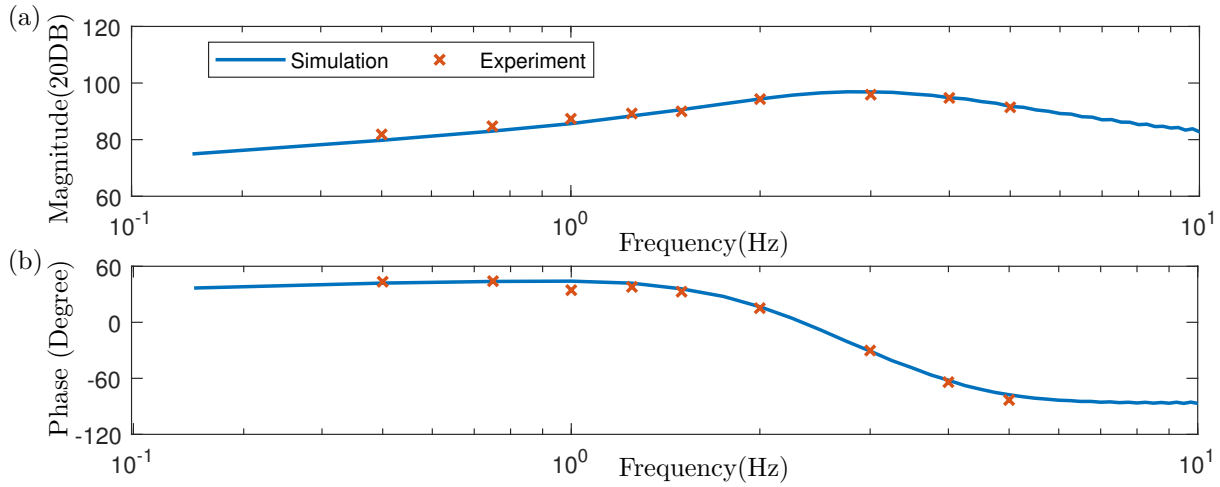

Figure 15: Theoretical and experimental results with identified effective stiffness from dynamic tests subjected to sinusoidal displacements with 5mm amplitude.

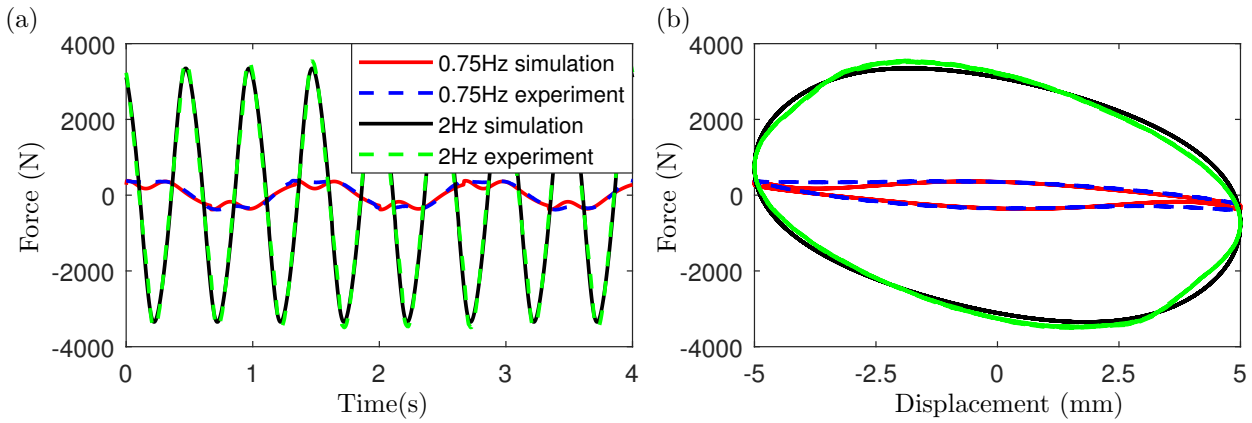

Figure 16: Force time histories (a) and hysteretic loops (b) of the fluid inerter prototype subjected to sinusoidal displacements with a 5 mm amplitude and 0.75 Hz, 2 Hz frequencies.

the identified parasitic effects on the performance, the mechanical model of the fluid inerter shown in Fig. 13 is used to replace the ideal inerter in $C2_3$ configurations. Note in this analysis, the inertance of the fluid inerter, defined in Eq. 20, is designed to be the optimum value reported in Table 1. As shown in Fig. 17, the mid-span displacements of the cable model subjected to the EI-centro earthquake and wind load are significantly enlarged compared to that of the ideal $C2_3$, even larger than that of the TMD for the wind load case.

To this end, the absorber $C2_3$ needs to be refined by re-optimising the component parameter values, including the stiffness k_1, the damping c_1 and the fluid inerter design. The design of fluid inerter involves seven parameters: $A_1,\ A_2,\ R,\ l,\ D_h,\ \rho,\ \mu$, where D_h is the tube diameter given by $D_h = \sqrt{4A_2/\pi}$. Previous works [70, 71] have described that the charateristic of fluid inerter is most sensitive to the three parameters, i.e. A_1, A_2 and l, hence the other parameters ($R,\ \rho,\ \mu$) are fixed to the values shown in Table 10. Since the parasitic effects of fluid inerter have nonlinear terms, for example the helical tube damping shown in Eq. (21), the performance matrix, the minimum damping ratio of the cable system is not applicable to select the optimal parameter values. In this optimisation, the root mean square value of the free decay midspan displacement with an initial condition

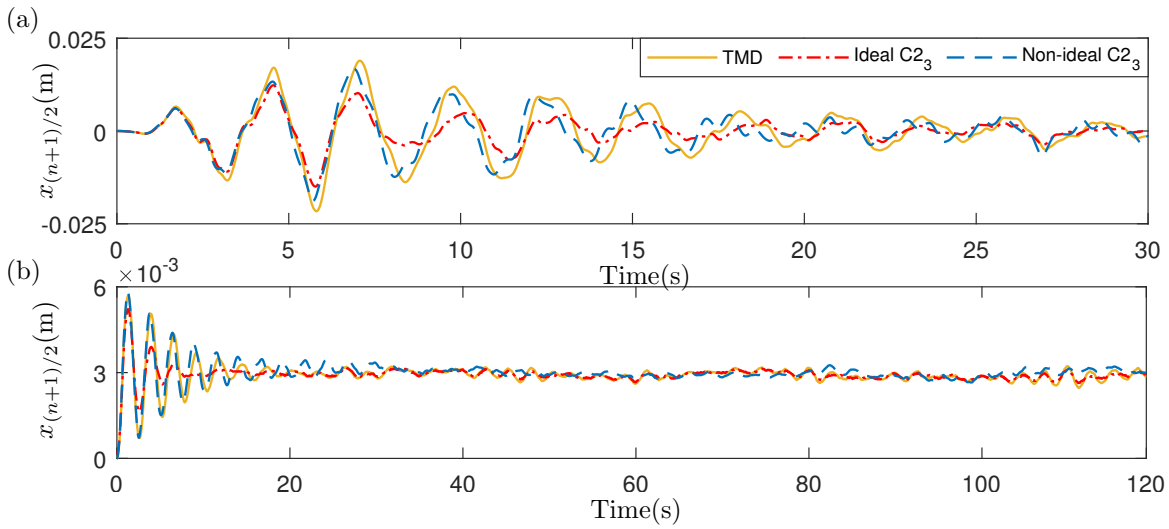

Figure 17: A comparison of the midspan displacement of the cable subjected to the EI-centro earthquake (a) and the wind load (b) with the TMD, the ideal $C2_3$ and the non-ideal $C2_3$ including the parasitic effects.

of 0.01m is selected as the objective function, and the optimum parameter values are shown in Table 11. The performance of the cable subjected to the earthquake excitations and the wind loads are also verified, for which the RMS and the maximum values of the midspan displacement with the refined $C2_3$ are calculated and illustrated in Table 11. By comparing with the optimized TMD, the performance improvements are also

Table 11: Optimum results of the refined $C2_3$ considering parasitic effects

Parameter values	$x_{(n+1)/2}$ $\times 10^{-3}$ (m)	Tohoku	Kobe	El-centro	Wind
$A_1 = 674.9\,\mathrm{cm}^2$, $A_2 = 28.9\,\mathrm{cm}^2$, $l = 16.6$ m, $c_1 = 3.1$ kNs/m, $k_1 = 91.9$ kN/m	RMS	2.40 (36.8%/ − 1.7%)	3.73 (17.1%/ − 0.8%)	3.89 (40.1%/ − 5.4%)	2.93 (1.4%/ − 0.7%)
	MAX	11.4 (42.4%/2.6%)	27.12 (17.3%/ − 3.8%)	15.10 (30.1%/ − 1.3%)	5.12 (10.2%/1.6%)

summarized in Table 11, suggesting that the vibration mitigation performance of the cable can be significantly improved by the non-ideal $C2_3$, with at most a 42.4% improvement for the Tohoku earthquake and at least a 17.1% improvement for the Kobe earthquake. Table 11 also presents a comparison of the performance between the ideal and non-ideal $C2_3$. It is found that the performance benefit of the ideal $C2_3$ is slightly reduced due to the introduction of more detailed parasitic effects, with up to 5.4% degradation. Taking the El-Centro earthquake excitation and wind loads as examples, the midspan displacement of the cable in the frequency domain is shown in Fig. 18, indicating the same conclusion as Table 11.

6. Conclusion

This study presents a systematic synthesis and optimisation framework for identifying tuned mass inerter absorbers for suppressing cable vibrations. A systematic approach was used to enumerate all the possible candidate layouts with a reaction mass and one inerter, one damper, one spring. Unlike existing studies

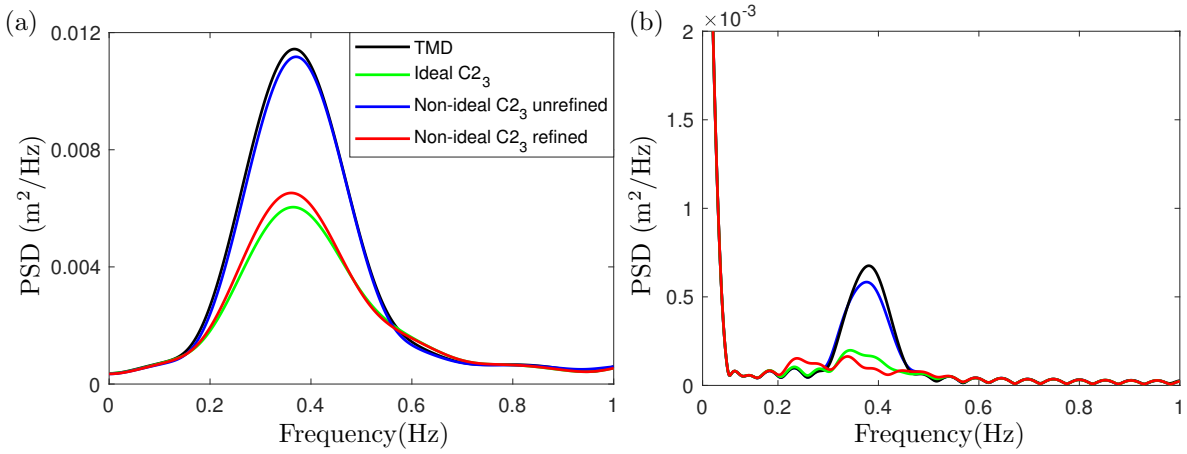

Figure 18: A comparison of the frequency domain midspan displacement of the cable subjected to the EI-centro earthquake (a) and the wind load (b) with the TMD, the ideal $C2_3$, the unrefined non-ideal $C2_3$ and the refined non-ideal $C2_3$.

that focus on a limited number of predefined absorber configurations, the proposed methodology enables a comprehensive exploration of the TMIA design space and provides a rational basis for identifying optimal absorber topologies. A finite element model of the cable was established, and the minimum damping ratio around the first fundamental frequency was selected as the performance measure for optimisation, where the damping ratio of up to four modes were also considered as the optimisation constraints. With the proposed method, two optimal tuned mass inerter absorbers with one attachment point and two attachment points were identified, termed as $C1$ and $C2_3$. It was found that the tuned mass inerter absorbers with two attachment points outperform those with one point and the optimum configuration, the $C2_3$, can provide approximately twice the first-mode damping ratio compared to the TMD. Robustness verification was also conducted to confirm that the proposed absorbers maintain vibration suppression effectiveness under changes in system parameters and locations.

To further evaluate the control capability of the proposed tuned mass inerter absorbers, earthquake excitations and wind loads generated using the Kaimal spectrum were adopted. The time-domain and the corresponding PSD of the cable midspan displacements were simulated, for which the maximum and root mean square values were calculated. The results indicated that the proposed tuned mass inerter absorber configurations apparently mitigate the midspan vibration amplitudes compared to the traditional absorbers, the TMD and the TMDI, under both the earthquake and wind loads. It has been shown that for the three earthquake excitations, the optimum $C2_3$ can reduce the maximum midspan displacements by up to 33.1% and 7.9% compared to the TMD and the TMDI. Considering the wind-induced vibrations, the $C2_3$ can provide approximately 8.8% and 4.2% smaller value of the maximum midspan response than the TMD and the TMDI, further illustrating the superior control effectiveness of the identified tuned mass inerter absorbers based on the proposed design methodology. In addition to the improved vibration mitigation performance, the optimal $C2_3$ configuration also requires a smaller absorber stroke than the conventional TMDI under the considered loading cases, indicating a favourable trade-off between control effectiveness and practical implementation requirements. Consider the physical realisation of the identified optimum absorber, a fluid inerter setup is adopted given that the spring and

damper components have been extensively developed and validated in engineering practice. The key parasitic effects of this setup are experimentally identified, and it is found that the parasitic effects significantly degrade the control effectiveness. It is also illustrated that by refining the parameter values of the identified absorber, the vibration suppression benefits are still preserved.

Although the proposed framework demonstrates promising performance, several limitations should be acknowledged. The present study adopts a simplified tension-dominated in-plane cable model and considers only stochastic along-wind excitation generated using the Kaimal spectrum. Consequently, the findings are most directly applicable to tension-dominated cables undergoing relatively small-amplitude vibrations. Future work will investigate the influence of different wind characteristics and develop more realistic cable–wind interaction models incorporating different wind directions, and extend the proposed framework to more complex cable models. Further experimental validation of the complete cable–TMIA system will also be pursued to support practical implementation of the proposed methodology.

Acknowledgement(s)

The authors would like to acknowledge the support of the Guangdong Basic and Applied Basic Research Foundation, China (Grant No. 2023A1515240037), Guangzhou Basic and Applied Basic Research Foundation (No. 2025A04J3839), National Natural Science Foundation of China (Grant No. 52008259) and the Guangdong Provincial Key Laboratory of Advanced Manufacturing Technology for Marine Energy Facilities, China (Grant No. 2023B1212010012).

References

[1] H. Zhang, H. Wang, Z. Xu, Z. Liu, G. H., Dynamic performance of ultra-long stay cable in small-scale extreme winds, Engineering Structures 290 (2023) 116369. doi:10.1016/j.engstruct.2023.116369.

[2] L. Sun, L. Chen, H. Huang, Stay cable vibration mitigation: A review, Advances in Structural Engineering 25 (2022) 3368–3404. doi:10.1177/13694332221132316.

[3] A. Radu, I. Lazar, S. Neild, A. Sextos, Risk assessment of cables vibration-suppressed with tuned-inerter dampers, Engineering Structures 222 (2020) 111127. doi:10.1016/j.engstruct.2020.111127.

[4] H. Jing, X. He, Z. Wang, Numerical modeling of the wind load of a two-dimensional cable model in rain–wind-induced vibration, Journal of Fluids and Structures 82 (2018) 121–133. doi:10.1016/j.jfluidstructs.2018.06.019.

[5] J. Panda, M. Chopra, V. Matsagar, S. Chakraborty, An iterative gradient descent-based reinforcement learning policy for active control of structural vibrations, Computers & Structures 290 (2024) 107183. doi:10.1016/j.compstruc.2023.107183.

[6] T. Yu, Z. Mu, E. Johnson, Real-time neural network based semiactive model predictive control of structural vibrations, Computers & Structures 275 (2023) 106899. doi:10.1016/j.compstruc.2022.106899.

[7] N. Tran, V. Hoang, H. Bui, H. Cao, Upgraded double tuned mass dampers for vibration control of structures under earthquakes, Computers & Structures 310 (2025) 107700. doi:10.1016/j.compstruc.2025.107700.

[8] H. Tabatabai, A. Mehrabi, Design of mechanical viscous dampers for stay cables, Journal of Bridge Engineering 5 (2000) 114–123. doi:10.1061/(ASCE)1084-0702(2000)5:2(114).

[9] S. Krenk, S. Nielsen, Vibrations of a shallow cable with a viscous damper, Proceedings of the Royal Society of London. Series A: Mathematical, Physical and Engineering Sciences 458 (2002) 339–357. doi:10.1098/rspa.2001.0879.

[10] J. Main, N. Jones, Free vibrations of taut cable with attached damper. ii: Nonlinear damper, Journal of Engineering Mechanics 128 (2002) 1072–1081. doi:10.1061/(ASCE)0733-9399(2002)128:10(1072).

[11] Z. Liu, R. Zhang, S. Zhou, C. He, L. Zeng, Y. Meng, Z. Chen, Suppression of multi-mode non-planar rain-wind-induced vibrations of stay cables: Scruton number threshold and optimal damper design, Journal of Wind Engineering and Industrial Aerodynamics 265 (2025) 106196. doi:10.1016/j.jweia.2025.106196.

[12] H. Zhou, L. Sun, F. Xing, Damping of full-scale stay cable with viscous damper: experiment and analysis, Advances in Structural Engineering 17 (2014) 265–274. doi:10.1260/1369-4332.17.2.265.

[13] E. Aydın, S. Dinçer, M. Turfan, Detection of strand natural frequencies and vibration levels using mems accelerometers before and after the installation of tuned mass dampers for a stayed cable bridge istanbul bridge conference (ibridge 2022) (2022).

[14] Y. Xu, Z. Xu, Y. Guo, M. Zhou, Y. Zhao, Y. Yang, J. Dai, J. Zhang, C. Zhu, B. Ji, Y. Du, Z. Chen, A programmable pseudo negative stiffness control device and its role in stay cable vibration control, Mechanical Systems and Signal Processing 173 (2022) 109054. doi:10.1016/j.ymssp.2022.109054.

[15] J. Li, J. Shen, S. Zhu, Adaptive self-powered active vibration control to cable structures, Mechanical Systems and Signal Processing 188 (2023) 110050. doi:10.1016/j.ymssp.2022.110050.

[16] D. Qian, Y. Cong, H. Kang, X. Su, Dynamics on vortex-induced vibration suppression of a flexible cable by tuned mass damper, Communications in Nonlinear Science and Numerical Simulation 151 (2025) 109129. doi:10.1016/j.cnsns.2025.109129.

[17] A. Acampora, J. Macdonald, C. Georgakis, N. Nikitas, Identification of aeroelastic forces and static drag coefficients of a twin cable bridge stay from full-scale ambient vibration measurements, Journal of Wind Engineering and Industrial Aerodynamics 124 (2014) 90–98. doi:10.1016/j.jweia.2013.10.009.

[18] K. Bakis, M. Massaro, M. Williams, J. Graham, Passive control of bridge wind-induced instabilities by tuned mass dampers and movable flaps, Journal of Engineering Mechanics 143 (2017) 04017078. doi:10.1061/(ASCE)EM.1943-7889.0001287.

[19] C. Cai, W. Wu, X. Shi, Cable vibration reduction with a hung-on tmd system. part i: Theoretical study, Journal of Vibration and Control 12 (2006) 801–814. doi:10.1177/1077546306065857.

[20] V. Cu, B. Han, A stay cable with viscous damper and tuned mass damper, Australian Journal of Structural Engineering 16 (2015) 316–323. doi:10.1080/13287982.2015.1092693.

[21] F. Di, L. Sun, L. Chen, Suppression of vortex-induced high-mode vibrations of a cable-damper system by an additional damper, Engineering Structures 242 (2021) 112495. doi:10.1016/j.engstruct.2021.112495.

[22] X. Yang, H. Zhou, C. Cai, X. Huang, Y. Du, Vibration damping of a taut cable with the hybrid application of a viscous damper and a tuned mass damper, Journal of Bridge Engineering 29 (2024) 04024014. doi:10.1061/JBENF2.BEENG-6411.

[23] H. Li, K. Bi, Q. Han, R. Ma, A state-of-the-art review on negative stiffness-based structural vibration control, Engineering Structures 323 (2025) 119247. doi:10.1016/j.engstruct.2024.119247.

[24] Z. Cheng, R. Ma, Z. Wang, X. Du, K. Bi, Effectiveness of a novel magnetic negative stiffness eddy-current damper for multi-mode vibration control of stay cables: Experimental and numerical investigations, Engineering Structures 346 (2026) 121582. doi:10.1016/j.engstruct.2025.121582.

[25] J. Song, K. Bi, R. Ma, Z. Wang, K. Xu, H. Hao, Vibration control of adjacent structures equipped with inerter-based dampers considering nonlinearities: Analytical and experimental studies, Mechanical Systems and Signal Processing 206 (2024) 110903. doi:10.1016/j.ymssp.2023.110903.

[26] J. Dai, Z. Xu, P. Gai, Z. Hu, Optimal design of tuned mass damper inerter with a maxwell element for mitigating the vortex-induced vibration in bridges, Mechanical Systems and Signal Processing 148 (2021) 107180. doi:10.1016/j.ymssp.2020.107180.

[27] M. Wei, J. Zhang, K. Sun, C. Chea, X. Zhang, Z. Liu, F. Jiang, Design, characterization, and simulation of a novel multi-stage inertial damper for wind turbine structural vibration control, Energy 347 (2026) 140407. doi:10.1016/j.energy.2026.140407.

[28] I. Lazar, S. Neild, D. Wagg, Vibration suppression of cables using tuned inerter dampers, Engineering Structures 122 (2016) 62–71. doi:10.1016/j.engstruct.2016.04.017.

[29] X. Shi, W. Shi, L. K., L. Xing, S. Zhu, Optimal design of tuned inerter dampers with series or parallel stiffness connection for cable vibration control, Structural Control and Health Monitoring 28 (2021) e2673. doi:10.1002/stc.2673.

[30] Y. Wen, Y. Zhao, L. Chen, Damping and tuning of inerter-based dampers for cable vibration mitigation considering girder vibrations, Engineering Structures 296 (2023) 116893. doi:10.1016/j.engstruct.2023.116893.

[31] L. Sun, J. Sun, S. Nagarajaiah, L. Chen, Inerter dampers with linear hysteretic damping for cable vibration control, Engineering Structures 247 (2021) 113069. doi:10.1016/j.engstruct.2021.113069.

[32] L. Chen, S. Nagarajaiah, L. Sun, A unified analysis of negative stiffness dampers and inerter-based absorbers for multimode cable vibration control, Journal of Sound and Vibration 494 (2021) 115814. doi:10.1016/j.jsv.2020.115814.

[33] Y. Li, W. Shen, H. Zhu, Vibration mitigation of stay cables using electromagnetic inertial mass dampers: Full-scale experiment and analysis, Engineering Structures 200 (2019) 109693. doi:10.1016/j.engstruct.2019.109693.

[34] Z. Wang, Z. Cheng, G. Yin, W. Shen, A magnetic negative stiffness eddy-current inertial mass damper for cable vibration mitigation, Mechanical Systems and Signal Processing 188 (2023) 110013. doi:10.1016/j.ymssp.2022.110013.

[35] J. Luo, J. Jiang, J. Macdonald, Cable vibration suppression with inerter-based absorbers, Journal of Engineering Mechanics 145 (2019) 04018134. doi:10.1061/(ASCE)EM.1943-7889.0001554.

[36] J. Luo, J. Macdonald, J. Jiang, Identification of optimum cable vibration absorbers using fixed-sized-inerter layouts, Mechanism and Machine Theory 140 (2019) 292–304. doi:10.1016/j.mechmachtheory.2019.06.008.

[37] H. Gao, H. Wang, J. Li, J. Mao, Z. Wang, Dynamic behavior and damping enhancement of cable with negative stiffness inerter damper, International Journal of Mechanical Sciences 235 (2022) 107664. doi:10.1016/j.ijmecsci.2022.107664.

[38] Y. Hu, M. Chen, Performance evaluation for inerter-based dynamic vibration absorbers, International Journal of Mechanical Sciences 99 (2015) 297–307. doi:10.1016/j.ijmecsci.2015.06.003.

[39] X. Bai, Q. Liang, L. Huo, Vibration control of beam-model using tuned inerter enhanced tmd, Journal of Sound and Vibration 510 (2021) 116304. doi:10.1016/j.jsv.2021.116304.

[40] S. Zhang, X. Sheng, J. Jiang, H. Zhou, W. Ren, Z. Zhang, Vibration suppression of bridges under moving loads using the structure-immittance approach, International Journal of Mechanical Sciences 211 (2021) 106792. doi:10.1016/j.ijmecsci.2021.106792.

[41] L. Marian, A. Giaralis, Optimal design of a novel tuned mass-damper–inerter (tmdi) passive vibration control configuration for stochastically support-excited structural systems, Probabilistic Engineering Mechanics 38 (2014) 156–164. doi:10.1016/j.probengmech.2014.03.007.

[42] M. Akbari, T. Falborski, R. Jankowski, A novel hybrid seismic control system utilizing the acceleration differential force between a base-isolated building and an active tuned mass damper inerter under near-field excitations, Archives of Civil and Mechanical Engineering 26 (2) (2026) 43. doi:10.1007/s43452-025-01406-0.

[43] M. Akbari, T. Falborski, R. Jankowski, Optimal design tid controller with filter for multi-storey buildings equipped with active tendons and double-tuned mass damper inerter under near-field earthquakes, Journal of Building Engineering 111 (2025) 113244. doi:10.1016/j.jobe.2025.113244.

[44] M. Akbari, T. Falborski, R. Jankowski, Evaluating optimal inerter location for tuned mass damper inerter systems in multi-storey buildings considering ssi effects, Mechanical Systems and Signal Processing 232 (2025) 112734. doi:10.1016/j.ymssp.2025.112734.

[45] A. Giaralis, A. Taflanidis, Optimal tuned mass-damper-inerter (tmdi) design for seismically excited mdof structures with model uncertainties based on reliability criteria, Structural Control and Health Monitoring 25 (2018) e2082. doi:10.1002/stc.2082.

[46] X. Jin, M. Chen, Z. Huang, Minimization of the beam response using inerter-based passive vibration control configurations, International Journal of Mechanical Sciences 119 (2016) 80–87. doi:10.1016/j.ijmecsci.2016.10.007.

[47] O. Araz, M. A. Shahraki, Optimal design of a novel enhanced inerter-based tuned mass damper in seismic-excited structures considering ssi effects, Advances in Engineering Software 217 (2026) 104162. doi:10.1016/j.advengsoft.2026.104162.

[48] M. Calayir, J. Tao, O. Mercan, M. A. Bezabeh, Multi-hazard wind-seismic vibration mitigation of tall buildings using tuned mass damper inerter (tmdi) and structural modification: Numerical optimization and experimental validation, Earthquake Engineering & Structural Dynamics 55 (2026) 1071–1095. doi:10.1002/eqe.70129.

[49] M. A. Shahraki, O. Araz, Energy-based wind vibration control of turbines equipped with nonlinear tuned mass damper inerter considering soil-structure interaction, Proceedngs of The Institution of Mechanical Engineers Part A-Journal of Power and Energy (2025) 09576509251412557doi:10.1177/09576509251412557.

[50] H. He, Y. Zhou, P. Tan, Y. Xiang, L. Liu, X. Luo, Performance enhancement of existing tuned mass damper (tmd) via an optimally designed tuned inerter damper for seismic application, Engineering Structures 353 (2026) 122299. doi:10.1016/j.engstruct.2026.122299.

[51] O. Araz, Performance evaluation and optimization of nontraditional inerter-based tuned mass damper for seismic control of multi-story buildings considering ssi effects 81 (2025) 110350. doi:10.1016/j.istruc.2025.110350.

[52] S. Zhang, Y. Li, J. Jiang, S. Neild, H. Macdonald, A methodology for identifying optimum vibration absorbers with a reaction mass, Proceedings of the Royal Society A 475 (2019) 20190232. doi:10.1098/rspa.2019.0232.

[53] S. Zhang, J. Jiang, S. Neild, Passive vibration control: a structure–immittance approach, Proceedings of the Royal Society A: Mathematical, Physical and Engineering Sciences 473 (2017) 20170011. doi:10.1098/rspa.2017.0011.

[54] M. Smith, Synthesis of mechanical networks: the inerter, IEEE Transactions on automatic control 47 (2002) 1648–1662. doi:10.1109/TAC.2002.803532.

[55] Y. Li, Z. Cheng, N. Hu, Y. Yang, Z. Yin, Study of dynamic breakdown of inerter and the improved design, Mechanical Systems and Signal Processing 167 (2022) 108520. doi:10.1016/j.ymssp.2021.108520.

[56] A. Pirrotta, N. Di, A. Leonardo, C. Masnata, Theoretical and experimental investigation on an improved rack and pinion inerter, Nonlinear Dynamics (2024) 1–22doi:10.1007/s11071-024-10532-y.

[57] X. Liu, J. Jiang, B. Titurus, A. Harrison, Model identification methodology for fluid-based inerters, Mechanical Systems and Signal Processing 106 (2018) 479–494. doi:10.1016/j.ymssp.2018.01.018.

[58] M. Chillemi, T. Furtmüller, C. Adam, A. Pirrotta, Nonlinear mechanical model of a fluid inerter, Mechanical Systems and Signal Processing 188 (2023) 109986. doi:10.1016/j.ymssp.2022.109986.

[59] M. Chillemi, T. Furtmüller, C. Adam, A. Pirrotta, Experimental and numerical investigation of a fluid inerter for structural control, Journal of Sound and Vibration 573 (2024) 118222. doi:10.1016/j.jsv.2023.118222.

[60] M. Chillemi, T. Furtmüller, C. Adam, A. Pirrotta, Fluid inerter-based vibration control of multi-modal structures subjected to vertical vibration, Engineering Structures 307 (2024) 117938. doi:10.1016/j.engstruct.2024.117938.

[61] Y. Shen, Y. Liu, L. Chen, X. Yang, Optimal design and experimental research of vehicle suspension based on a hydraulic electric inerter, Mechatronics 61 (2019) 12–19. doi:10.1016/j.mechatronics.2019.05.002.

[62] S. Krenk, Vibrations of a taut cable with an external damper, Journal of Applied Mechanics 67 (2000) 772–776. doi:10.1115/1.1322037.

[63] D. Nguyen, D. Vo, M. Haque, Theoretical investigation on the impact of two hdr dampers on first modal damping ratio of stay cable, Applied Sciences 11 (2021) 10985. doi:10.3390/app112210985.

[64] W. Wu, C. Cai, Theoretical exploration of a taut cable and a tmd system, Engineering structures 29 (2007) 962–972. doi:10.1016/j.engstruct.2006.07.009.

[65] M. Javanbakht, S. Cheng, F. Ghrib, Multimode vibration control of stay cables using optimized negative stiffness damper, Structural Control and Health Monitoring 27 (2020) e2503. doi:10.1002/stc.2503.

[66] H. Wang, R. Hu, J. Xie, T. Tong, A. Li, Comparative study on buffeting performance of sutong bridge based on design and measured spectrum, Journal of Bridge Engineering 18 (2013) 587–600. doi:10.1061/(ASCE)BE.1943-5592.0000394.

[67] S. Peng, L. Zhang, Y. Chen, X. Chai, Experimental study on the performance of tuned mass damper inerter in suppressing low-frequency vibrations of long-span bridges: Model experiments and full-scale field tests, Structures 73 (2025) 108357. doi:10.1016/j.istruc.2025.108357.

[68] B. Wang, F. Xu, M. Zhang, Experimental and numerical study of a novel low-frequency tuned mass damper-inerter, Engineering Structures 331 (2025) 119980. doi:10.1016/j.engstruct.2025.119980.

[69] L. Ljung, System Identification: Theory for the user, New Jersey: Prentice-Hall Inc., 1987.

[70] D. Domenicoa, P. Deastra, G. Ricciardi, N. Sims, D. Wagg, Novel fluid inerter based tuned mass dampers for optimised structural control of base-isolated buildings, Journal of the Franklin Institute 356 (2019) 7626–7649. doi:10.1016/j.jfranklin.2018.11.012.

[71] P. Deastra, D. Wagg, N. Sims, The realisation of an inerter-based system using fluid inerter, Dynamics of Civil Structures 2 (2019) 127–134. doi:10.1007/978-3-319-74421-6_16.

DSPACE

https://dspace.org/

Configuration optimisation of tuned mass inerter absorbers for cable vibration suppression considering experimentally identified parasitic effects

Zhang, Sara Ying; Li, Deyuan; Zhu, Qi; He, Haonan; Li, Yiyuan

2026-09
Elsevier
https://doi.org/10.1016/j.compstruc.2026.108344
Zhang SY, Li D, Zhu Q, et al., (2026) Configuration optimisation of tuned mass inerter absorbers for cable vibration suppression considering experimentally identified parasitic effects. Computers & Structures, Volume 330, September 2026, Article number 108344

Downloaded from a DSpace repository. https://dspace.org/